


# Petrogenesis of the Ultramafic Zone of the Stillwater Complex in North America: constraints from mineral chemistry and stable isotopes of Li and O

Ben-Xun Su<sup>1,2,3</sup>  · Yang Bai<sup>1,2,3</sup> · Meng-Meng Cui<sup>1,2,3</sup> · Jing Wang<sup>1,2,3</sup> · Yan Xiao<sup>2,4</sup> · Davide Lenaz<sup>5</sup> · Patrick Asamoah Sakyi<sup>6</sup> · Paul T. Robinson<sup>1</sup>

Accepted: 11 June 2020

## Abstract

To investigate the petrogenesis of cyclic units in layered intrusions, we examined chromitite, dunite, poikilitic harzburgite and bronzitite from the Ultramafic Zone of the Stillwater Complex and measured stable isotopes of Li and O in their major minerals. The Li isotopes in olivine range from 4 to 26‰ in  $\delta^7\text{Li}$  with uniform Li contents of 1–3 ppm, whereas orthopyroxene and clinopyroxene have Li contents of 0.5–5 ppm and 4–8 ppm, and  $\delta^7\text{Li}$  ranges of –13 to 7‰ and –14 to –6‰, respectively. The  $\delta^{18}\text{O}$  values vary from 4.91 to 5.72‰ in olivine, from 5.11 to 5.87‰ in orthopyroxene, and from 4.64 to 5.86‰ in clinopyroxene. For a given sample, olivine displays more variable and higher  $\delta^7\text{Li}$  but lower  $\delta^{18}\text{O}$  values than orthopyroxene, indicating that olivine experienced more extensive compositional modification after crystallization relative to orthopyroxene. The general Li and O isotopic compositions are interpreted as the result of re-equilibration between interstitial liquids, from which pyroxenes crystallized, and cumulus minerals. The inter-mineral and inter-sample isotopic variations correlate with mineral assemblages, crystal sizes and major and trace element compositions, revealing that the interstitial liquids varied compositionally mainly due to mixing between fractionated magma and newly injected primitive magma. Abrupt mineralogical and geochemical changes from silicate rocks to chromitites imply that hydrous fluids, which collected on chromite surfaces and were later released from chromite seams, played an additional, critical medium of chemical exchange between minerals in the chromitites.

**Keywords** Li isotopes · Oxygen isotopes · Chromite · Olivine · Pyroxene · Layered intrusion

## Introduction

It has been suggested that parental magmas of large mafic–ultramafic layered intrusions worldwide vary in composition due to different mixing proportions, consequently leading to chemical disequilibrium between the magmas and crystallizing minerals (e.g., Bushveld, Mondal and Mathez

---

Communicated by Daniela Rubatto.

---

✉ Ben-Xun Su  
subenxun@mail.iggcas.ac.cn

<sup>1</sup> Key Laboratory of Mineral Resources, Institute of Geology and Geophysics, Chinese Academy of Sciences, Beijing 100029, China

<sup>2</sup> Innovation Academy for Earth Science, Chinese Academy of Sciences, Beijing 100029, China

<sup>3</sup> University of Chinese Academy of Sciences, Beijing 100049, China

<sup>4</sup> State Key Laboratory of Lithospheric Evolution, Institute of Geology and Geophysics, Chinese Academy of Sciences, Beijing 100029, China

<sup>5</sup> Department of Mathematics and Geosciences, University of Trieste, Via Weiss 8, 34127 Trieste, Italy

<sup>6</sup> Department of Earth Science, University of Ghana, P.O. Box LG 58, Legon-Accra, Ghana

2007; Stillwater, McCallum 1996, 2002). This results in compositional variations and modifications in minerals via re-equilibration and interaction (Pagé et al. 2011). Further interaction or chemical diffusion may also occur between crystallized minerals and interstitial liquids (Raedeke and McCallum 1984; Lenaz et al. 2012) and between subsolidus mineral phases, such as olivine and chromite during solidification and cooling (Jackson 1961; McCallum 2002; Bai et al. 2019). The extent of such interactions depends largely on the spatial migration of the melts; O’Driscoll et al. (2009) proposed downward infiltration of a melt during the formation of layers in such intrusions, whereas others have argued for upward-percolation of the melts (Kaufmann et al. 2018) owing to compaction of the underlying crystal pile (Irvine 1980) or a temperature gradient-driven flux (Latypov et al. 2008). Thus, the cooling and crystallization history of large layered intrusions is long, complex, and involves multiple injections of primitive magma into an evolving and fractionating magma chamber. These processes would have modified the primary melt compositions and the constituent minerals, making it difficult to identify a clear parental magma. Moreover, much of the mineralogical evidence for mineral-interstitial melt interactions would likely have been obliterated during late post-magmatic textural maturation and recrystallization (Pagé et al. 2011). These considerations have led to several hypotheses for the formation of stratiform chromitite layers in layered intrusions including magma mixing (Irvine 1975; Horan et al. 2001; Spandler et al. 2005), mechanical sorting (Cooper 1990; Mondal and Mathez 2007; Maier et al. 2012; Mungall et al. 2016; Jenkins and Mungall 2018), fluid immiscibility (McDonald 1965; Spandler et al. 2005) and incongruent melting (Boudreau 2016).

Because lithium (Li) and incompatible trace elements are sensitive to changing magma compositions, fluid activity and limited Li diffusion between silicates and chromite

(Lambert and Simmons 1987; Eiler et al. 1995; Su et al. 2016, 2018; Tomascak et al. 2016), integration of such data and oxygen (O) isotopes may shed new light on the formation of large layered mafic–ultramafic intrusions. In this study, we conducted in situ analyses of major and trace elements and Li and O isotopes of major silicate minerals from the Ultramafic Zone of the Stillwater Complex following petrographical and mineralogical investigations. These datasets, together with the Cr isotope data from the same samples in Bai et al. (2019), are used to identify elemental and isotopic variations in different rock types and to constrain potential melt/fluid activity as well as chemical interactions between various components.

## Geology of the Stillwater Complex

The 2.7-Ga Stillwater Complex was emplaced into Archean meta-sedimentary rocks on the northern margin of the Wyoming Craton (Fig. 1a) (Jones et al. 1960; McCallum 1996). It has an exposed strike length of ~45 km (Fig. 1b) and a maximum thickness of 6.5 km (Jackson 1961). The Stillwater Complex has been divided into three major stratigraphic zones based on lithology and mineralogy, named in order from the bottom upward: the Basal Zone, the Ultramafic Zone and the Banded Zone (McCallum 1996). The Basal Zone, which is composed chiefly of diabasic norite with minor local harzburgite, separates the complex from its footwall country rocks (McCallum 2002). This zone commonly contains sulfide grains and patches of pyrrhotite and chalcopyrite (Peoples and Howland 1940; Aird et al. 2017). The Ultramafic Zone may be subdivided into two subzones (Zientek et al. 1985). The lower peridotite subzone is characterized by lithologically similar, cyclic units of olivine-chromite-orthopyroxene layers (Raedeke and McCallum

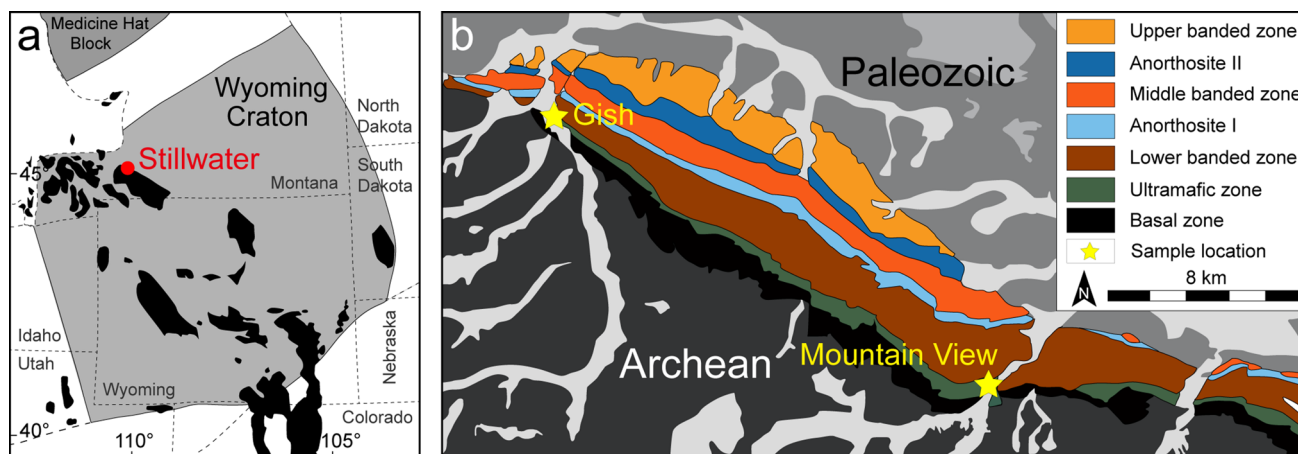


**Fig. 1** a Distribution of Precambrian basement (in black) and location of the Stillwater Complex in the Wyoming Craton, and (b) geologic map of the Stillwater Complex (after Jackson 1961)

1984; Cooper 1997; Lenaz et al. 2012). The upper bronzitite subzone consists almost exclusively of medium- to coarse-grained bronzitite. The overlying Banded Zone is composed of norite, gabbro-norite and gabbro, to troctolite and anorthosite (McCallum 2002). The top of the intrusion is eroded and overlain unconformably by Cambrian sedimentary rocks.

The chromite deposits occur as massive layers and as disseminations near the lower half of the Ultramafic Zone and are referred to as A through K (Campbell and Murck 1993). The chromitites in the Ultramafic Zone are interlayered with poikilitic harzburgite, and bronzitite and dunite (Jackson 1970; Cooper 1997) (Fig. 2a–c), whereas those in the Banded Zone occur as disseminated bodies in olivine-bearing rocks and as rare chromite-rich seams associated with thin anorthosites. The (semi-)massive chromitite generally shows sharp contacts with disseminated or anti-nodular chromitite and then gradually grades into poikilitic harzburgite and bronzitite (Fig. 2a, d). Chromitite seams may also bifurcate, splitting and joining with other seams along strike (Fig. 2d), similar to bifurcations in the Bushveld Complex (Pebane and Latypov 2017). The poikilitic harzburgite may locally replace the granular harzburgite as shown by the presence of poikilitic fingers intruding into the granular harzburgite (Boudreau 2016).

## Sample descriptions

The samples in this study were collected mainly from the peridotite subzone of the Ultramafic Zone. Six samples were collected from the cyclic chromitite unit of seam G in the Mountain View section, and seven samples were collected

from the unmineralized lowermost cyclic unit in the Gish area (Figs. 1b, 3a; Supplementary Table S1). One basal harzburgite sample was also collected from the contact between the Basal Zone and the Ultramafic Zone. The principal rock types vary from poikilitic harzburgite and dunite to chromitite and bronzitite (Fig. 3b–g). They are mostly composed of olivine, orthopyroxene and chromite with varying amounts of plagioclase and clinopyroxene. Plagioclase is absent or less abundant in the chromitites than in the harzburgites. Previous studies (Jones et al. 1960; Campbell and Murck 1993; Jenkins and Mungall 2018), and our Fig. 3, show that orthopyroxene, clinopyroxene, and plagioclase mainly occur as oikocrysts including olivine and chromite chadacrysts in the peridotite subzone of the Stillwater Complex. The crystallization sequence is olivine → chromite → orthopyroxene (→ plagioclase → clinopyroxene). Note that it is difficult to determine the crystallization order of the last two members of the sequence solely from the ultramafic rocks. There are some field outcrops and hand specimens in which plagioclase follows orthopyroxene and clinopyroxene follows plagioclase (Jackson 1961; McCallum 1996, 2002).

## Poikilitic harzburgite

Harzburgites in the Ultramafic Zone are coarse-grained rocks with either granular or poikilitic textures (Howland et al. 1949; Jones et al. 1960). The granular harzburgites comprise only a small stratigraphic proportion (Fig. 3a) and consist chiefly of olivine and pyroxene grains which may exceed 1 cm in length. Plagioclase, chromite, biotite and even apatite are locally present as interstitial accessory minerals (Howland et al. 1949). The poikilitic harzburgite occurs mostly in the peridotite subzone where it hosts most

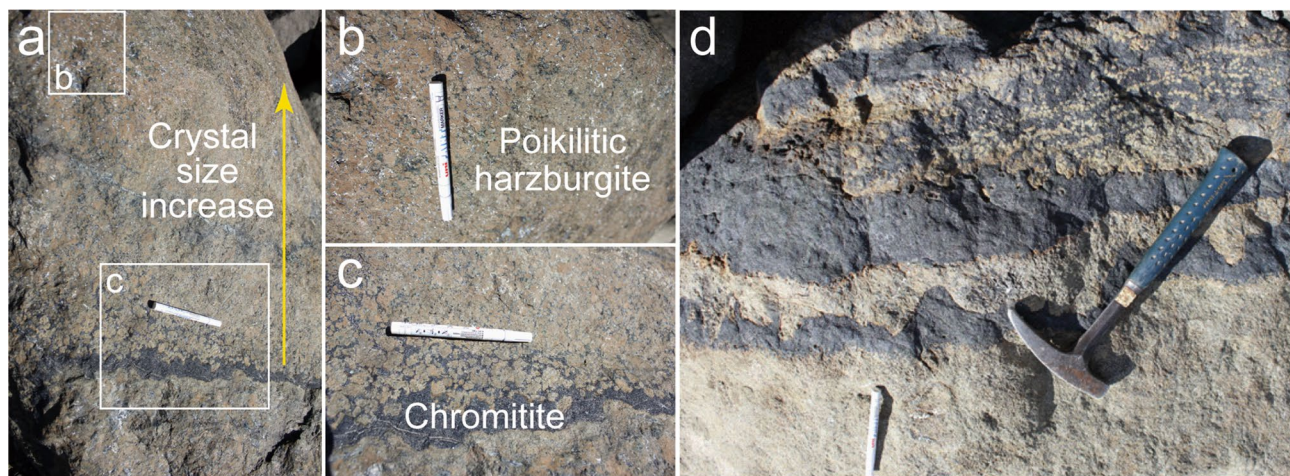


**Fig. 2** Field outcrops showing contacts between chromitite seams and silicate rocks and their crystal size variations. Massive chromitite shows sharp contacts with anti-nodular chromitite and then gradually

grades into poikilitic harzburgite (a), and average chromite crystal size increases uniformly upward (a–c). Chromitite seams may also bifurcate, splitting and joining with other seams along-strike (d)

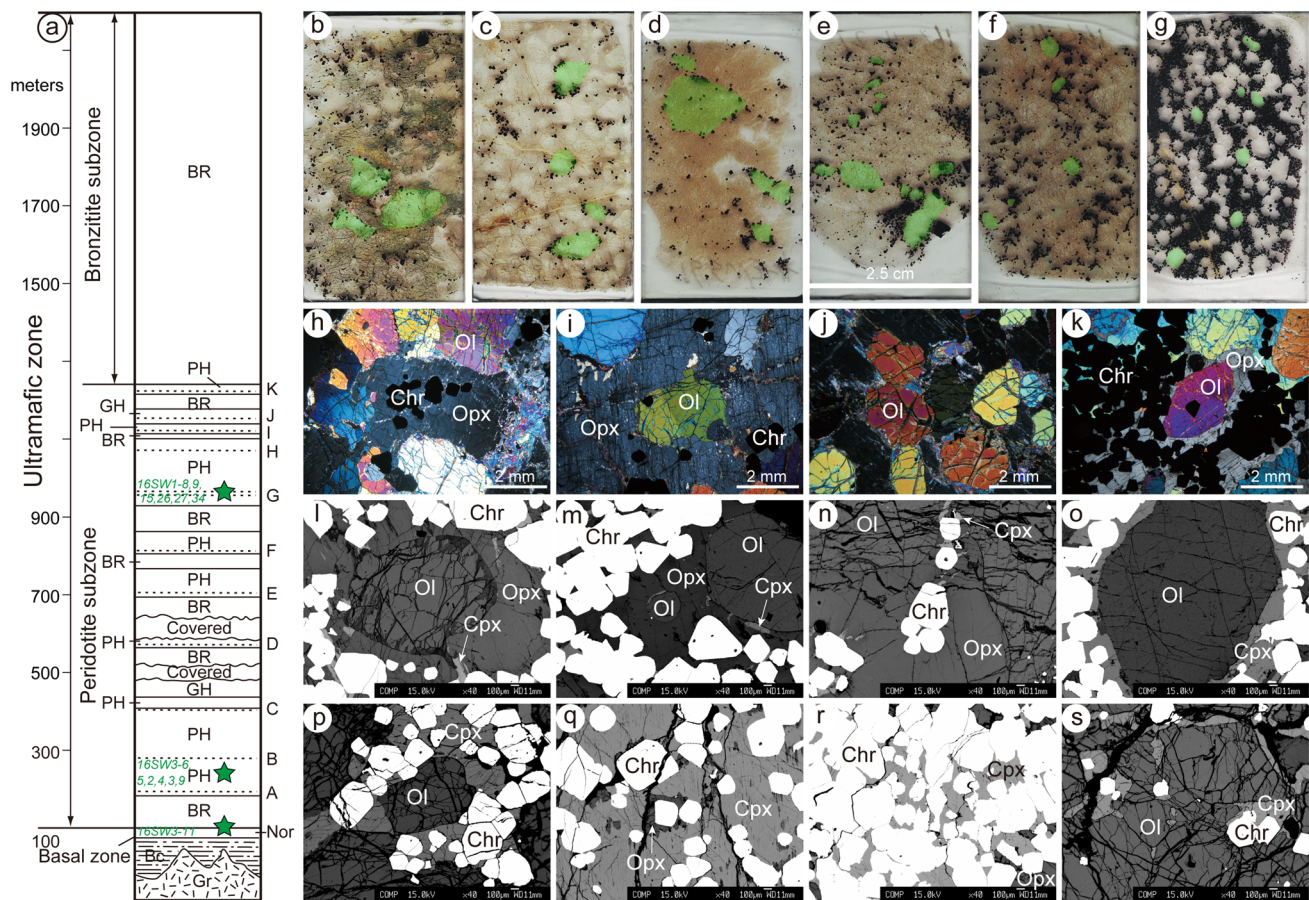


**Fig. 3** **a** Generalized columnar section of the Ultramafic Zone, eastern part of the Stillwater Complex (after McCallum 1996) with sample locations (star symbol). *BR* bronzitite, *Bc* basement complex, *Gr* granite, *GH* granular harzburgite, *Nor* norite, *PH* poikilitic harzburgite. **b–g** Scanned images of thin-sections of the Stillwater samples showing distribution and relation of minerals and general variations of crystal size from harzburgite (**b–c**) and dunite (**d–e**) to chromitite (**f–g**); **h** harzburgite sample 16SW1-5 showing chromite (Chr) enclosed in orthopyroxene (Opx); **i** harzburgite sample 16SW3-9 showing orthopyroxene poikilitic crystals enclosing rounded olivine (Ol); **j** dunite sample 16SW3-3 showing euhedral equigranular olivine; **k** chromitite sample 16SW1-8 showing euhedral chromite and rounded olivine grain within poikilitic orthopyroxene; **l** chromitite sample 16SW1-26 showing tiny clinopyroxene (Cpx) in orthopyroxene,

which encloses chromite and olivine; **m** chromitite sample 16SW1-8 showing olivine grains in variable size within orthopyroxene; **n** chromitite sample 16SW1-34 showing occurrence of euhedral chromite grains within olivine and orthopyroxene associated with minor clinopyroxene; **o** chromitite sample 16SW1-8 showing well-defined boundary between olivine and clinopyroxene; **p** chromitite sample 16SW1-9 showing clinopyroxene poikilitic crystal enclosing chromite and olivine and fracture development in chromite; **q** chromitite sample 16SW1-27 showing residual orthopyroxene poikilitic crystal in large clinopyroxene grain; **r** chromitite sample 16SW1-26 showing altered boundaries of chromite enclosed in clinopyroxene; **s** chromitite sample 16SW1-27 showing clinopyroxene-chromite association within or surrounding olivine

of the economic chromitites (Fig. 3a). This variety occurs on both sides of the chromite seams, and in some places, merges gradually into chromitite (Peoples and Howland 1940). The poikilitic harzburgites contain the same minerals as the granular varieties, but are characterized by relatively large, skeletal or poikilitic crystals enclosing rounded grains of olivine (Fig. 3h, i). Interstitial plagioclase is usually present and can constitute up to 15% of the rock, whereas small, black chromite grains are enclosed in both the plagioclase and orthopyroxene (Fig. 3i).

## Dunite

Dunite bodies, together with olivine-rich harzburgite and coarse-grained pyroxenite, typically occur in the lower part of the Ultramafic Zone, where they cut and locally obscure the primary layers of bronzitite and harzburgite (Peoples and Howland 1940; Jones et al. 1960). Gradations from dunite through harzburgite into layered bronzitite have also been observed in a few outcrops (Jones et al. 1960). Olivine crystals in the layered dunites studied here are variable in size

from mm to cm (Fig. 3d, e, j). Orthopyroxene crystals are present as skeletal oikocrystals making up a very small proportion of the rock. Chromite is ubiquitous in the dunites, whereas plagioclase is rare.

## Chromitite

In the Stillwater Complex, the chromite deposits are generally found with the poikilitic harzburgite (Peoples and Howland 1940; Jones et al. 1960) in the lower part of individual cyclic units. There are almost continuous gradations in places from nearly pure chromite to harzburgite with scattered chromite crystals (Jackson 1970; Cooper 1997). In chromitite, chromite and olivine are equigranular with various proportions (Fig. 3f, g), and orthopyroxene occurs as oikocrysts including olivine and chromite chadacrysts (Fig. 3k–n). Olivine grains are relatively uniform in grain size compared to those in the silicate rocks (Fig. 3g). Clinopyroxene may also be present as smaller poikilitic grains in some samples (Fig. 3o–r) or as swarm-like grains associated with chromite within orthopyroxene (Fig. 3l–n) or olivine (Fig. 3s). It should be noted that the chromite grains enclosed in clinopyroxene show well-developed fractures (Fig. 3p, q) and smoothed or poorly defined boundaries (Fig. 3o–r) relative to those in orthopyroxene. The silicate minerals are mostly well preserved in disseminated chromitites, whereas they are partially or completely serpentized in massive chromitites. It is also noticeable that olivine crystals in the studied samples are typically anhedral and exhibit peritectic texture with orthopyroxene rims (Fig. 3b–n) and rarely show direct contact with chromite. In addition, the chromitite layers are commonly associated with mafic pegmatite layers (Jones et al. 1960). Those pegmatites associated with the chromitite horizons are stratiform or locally cross-cut other layers, and they contain all combinations of minerals found in the Ultramafic Zone (Jenkins and Mungall 2018).

## Analytical methods

Olivine, orthopyroxene and clinopyroxene grains were hand-picked under a binocular microscope, and together with reference materials were mounted in epoxy. The mount was then polished to expose the crystals, which were identified using both transmitted and reflected light images. The minerals were first analyzed for major elements using an electron probe microanalyzer (EPMA) followed by oxygen and then Li isotopes with a Cameca IMS-1280 secondary ion mass spectrometry (SIMS). Finally, trace elements were measured using laser ablation inductively coupled plasma mass spectrometry (LA-ICP-MS). The same spots of the mineral grains were selected for all measurements to yield corresponding element and isotope data. All analyses were

conducted at the Institute of Geology and Geophysics, Chinese Academy of Sciences.

The major element analyses were carried out using a JEOL JXA8100 EPMA at an accelerating voltage of 15 kV and 10 nA beam current, 5  $\mu\text{m}$  beam spot and 10–30 s counting time on peak. Natural and synthetic mineral standards were used for calibration. A program based on the ZAF procedure was used for matrix corrections. Typical analytical uncertainty for all of the elements analyzed was better than 1.5%.

The SIMS oxygen isotope analyses of minerals were conducted using  $\text{Cs}^+$  ions as a primary beam with  $\sim 10 \mu\text{m}$  diameter, and  $\sim 2 \text{ nA}$  in intensity. The  $^{16}\text{O}$  and  $^{18}\text{O}$  ions are detected simultaneously by two faraday cups, and the signals were amplified by 10E10 ohm and 10E11 ohm resistors, respectively. A normal electron gun was used to compensate for the charging effect in the bombarded area. The entrance slit was set at  $\sim 120 \mu\text{m}$ ; the field aperture at  $6000 \times 6000 \mu\text{m}^2$ ; the energy slit at 40 eV, and the exit slit at  $\sim 500 \mu\text{m}$ . The magnification of the transfer system was configured as  $\sim 133$ . Each analysis consisted of pre-sputtering, beam centering, and signal collecting. The collecting process consisted of 16 cycles, each of which took 4 s. The  $^{18}\text{O}/^{16}\text{O}$  ratios were normalized to VSMOW and expressed as  $\delta^{18}\text{O}$ . Standards used to correct instrument mass fractionation included olivine 06JY06OL ( $\delta^{18}\text{O} = 5.20\text{‰}$ ), orthopyroxene 06JY34OPX ( $\delta^{18}\text{O} = 5.64\text{‰}$ ) and clinopyroxene 06JY31CPX ( $\delta^{18}\text{O} = 5.19\text{‰}$ ) (Tang et al. 2019). Detailed analytical procedures are described by Li et al. (2010) and Tang et al. (2015, 2019).

After the oxygen isotope analyses, the same mount was again polished to remove the analytical spots and vacuum-coated with high-purity gold for Li isotope analyses. The O-primary ion beam was accelerated at 13 kV, with an intensity of about 15–30 nA. The elliptical spot was approximately  $20 \times 30 \mu\text{m}$  in size. Positive secondary ions were measured on an ion multiplier in pulse counting mode, with a mass resolution (M/DM) of 1500 and an energy slit open at 40 eV without any energy offset. A 60-s pre-sputtering with raster was applied before analysis. The secondary ion beam position in apertures, as well as the magnetic field and the energy offset, were automatically centered before each measurement. Eighty cycles were measured with counting times of 7 and 2 s for  $^6\text{Li}$  and  $^7\text{Li}$ , respectively. The measured  $\delta^7\text{Li}$  values are given as  $\delta^7\text{Li}$  ( $[(^7\text{Li}/^6\text{Li})_{\text{sample}} / (^7\text{Li}/^6\text{Li})_{\text{L-SVEC}} - 1] \times 1000$ ) relative to units of the standard NIST SRM 8545 (L-SVEC) with  $^7\text{Li}/^6\text{Li}$  of 12.0192. The same standards as in oxygen isotope analyses were used to correct instrument mass fractionation. The olivine standard 06JY06OL has a Mg# ( $100 \times \text{Mg}/(\text{Mg} + \text{Fe})$ ) value of 89.6, Li concentration of 2.23 ppm and  $\delta^7\text{Li}$  of 5.34‰; the orthopyroxene standard 06JY34OPX has a Mg# of 92.1, Li concentration of 1.07 ppm and  $\delta^7\text{Li}$  of  $-0.77\text{‰}$ ; and the

clinopyroxene standard 06JY31CPX has a Mg# of 91.1, Li concentration of 1.16 ppm and  $\delta^7\text{Li}$  of  $-2.37\text{‰}$  (Su et al. 2015). Lithium concentrations of the samples were calculated on the basis of  $^7\text{Li}^+$  count rates (cps/nA) relative to the standard. The detection limit of Li was  $<1$  ppb and uncertainties were mostly  $<0.90$  ppm ( $1\sigma$ ). The internal errors of the Li isotopic compositions for both the standard and the olivine samples are less than  $1.20\text{‰}$  ( $1\text{se}$ ). Matrix effects, in which  $\delta^7\text{Li}$  increases by  $1.0\text{‰}$  for each mole percent decrease in the Mg# of olivine (Su et al. 2015), were considered for calibration. Detailed analytical procedures are described in Su et al. (2015, 2018).

After removing the gold coating on the mount, trace element compositions were determined with a 193 nm Coherent COMPex Pro ArF Excimer laser coupled to an Agilent 7500a ICP-MS. Each analysis was performed using 80  $\mu\text{m}$ -diameter ablating spots at 6 Hz with an energy of  $\sim 100$  mJ per pulse for 45 s after measuring the gas blank for 20 s. Reference materials NIST610 and NIST612 were used as external standards to produce calibration curves. Every eight analyses were followed by two analyses of the standards to correct for time-dependent drift. Calibration was performed using NIST612 as an external standard. Offline data processing was performed with the GLITTER 4.0 program using Mg for olivine and Si for orthopyroxene and clinopyroxene as internal standards, which were obtained by EPMA and shown in Supplementary Table S2.

## Results

All the rocks studied here are from the layer of poikilitic harzburgite containing chromite layer G (Fig. 3). The samples include five chromitites and one harzburgite from the G chromitite layer and four harzburgites and two dunites from the silicate layer of the lower part of the peridotite subzone and its contact with basal zone (referred to as the lowermost layer). Mineral compositional differences among the samples (Figs. 4, 5, 6) basically reflect variations between these two layers.

### Major and trace elements

Elemental compositions of olivine, orthopyroxene and clinopyroxene in the rocks from the Stillwater Complex are illustrated in Fig. 4. Olivine and orthopyroxene in silicate rocks from the lowermost layer have lower Mg# values of 84–85 and 84–87, respectively, than those in the G chromitite (olivine Mg# = 86–89; orthopyroxene Mg# = 87–91), whereas clinopyroxene in chromitites has higher Mg# values of 89–92 (Supplementary Table S2). These Mg# values overlap those of published datasets from the Stillwater Complex (Raedeke and McCallum 1984; Campbell and Murck 1993;

McCallum 2002). The Li contents in olivine are relatively uniform in a range of 1–3 ppm; orthopyroxene shows highly variable Li contents from 0.5 to 5 ppm, with the lowest contents in orthopyroxene from the chromitite samples. Clinopyroxene grains in the three analyzed chromitite samples have the highest Li contents of 4–8 ppm (Supplementary Table S2).

Transition elements in both olivine and orthopyroxene are distinctly different between the lowermost silicate layer and the G chromitite. The chromitites have overall larger variations and higher Ni concentrations in olivine and orthopyroxene than their counterparts in the harzburgites and dunites, whereas Mn, Co and Ti concentrations are lower (Fig. 4). Cr concentrations in both olivine and orthopyroxene overlap values in different rock types. The basal harzburgite and bronzitite samples commonly display maximum or minimum concentrations in these transition elements as well as in Mg# and Li content. In addition, olivine in chromitite has clearly higher Al contents than those in harzburgite and dunite, whereas Al concentrations in orthopyroxene show large inter- and intra-sample variations in all rock types (Fig. 4).

Trace element concentrations of orthopyroxene obtained in this study (Supplementary Table S2) are at the same levels as those in the Ultramafic Zone of the Stillwater Complex (Lambert and Simmons 1987) and those from the chromitite layers of the Bushveld Complex as given in Kaufmann et al. (2018) and Yang et al. (2019). Briefly, all these orthopyroxene crystals are characterized by relative enrichment in the heavy rare earth elements (HREE) relative to the light rare earth elements (LREE) and show large LREE variations (Fig. 5a, b). Orthopyroxene grains in the harzburgites and bronzitites (Fig. 5a) show remarkably negative Eu anomalies, as noted in the literature (Lambert and Simmons 1987), whereas grains in the dunites and chromitites show no or weakly negative Eu anomalies (Fig. 5b). The LREE concentrations of orthopyroxene are most enriched in bronzitite, the most depleted and variable in chromitite, and moderate in harzburgite and dunite. Clinopyroxene grains from the three chromitite samples show flat REE patterns with uniform LREE concentrations relative to HREE and slightly positive or negative Eu anomalies (Fig. 5c), which are similar to those in chromitite from the Bushveld Complex (Yang et al. 2019).

### Li and O isotopic compositions

Lithium isotopic compositions are highly variable with a decreasing  $\delta^7\text{Li}$  order of olivine ( $4\text{--}26\text{‰}$ )  $>$  orthopyroxene ( $-13$  to  $7\text{‰}$ )  $>$  clinopyroxene ( $-14$  to  $-6\text{‰}$ ). The dunites and harzburgites from the lowermost layer and one harzburgite sample from the G chromitite have overlapping  $\delta^7\text{Li}$  ranges in olivine and restricted  $\delta^7\text{Li}$  variations in orthopyroxene, considerably higher than their counterparts

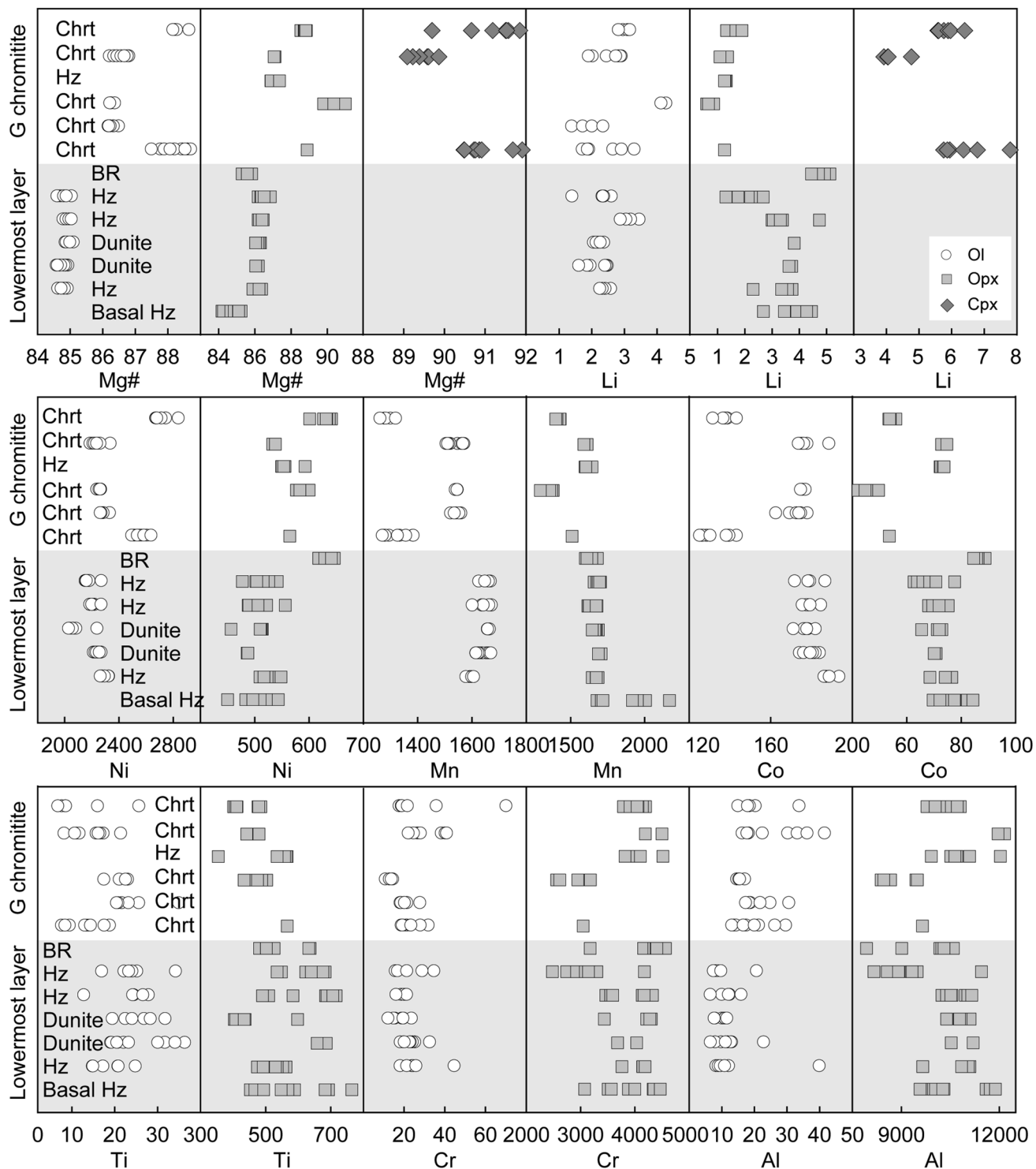
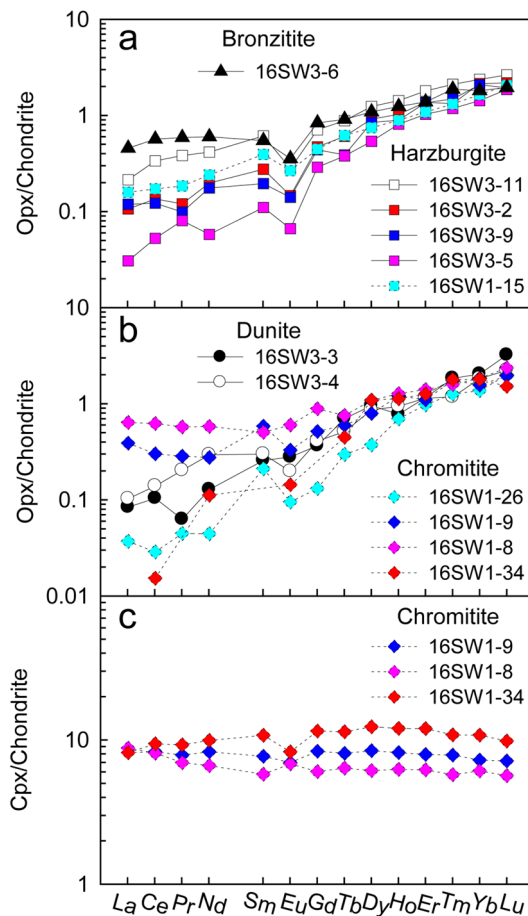


Fig. 4 Major and trace element compositions of minerals in the stratigraphic section of the Ultramafic Zone of the Stillwater Complex. *BR* bronzitite, *Chrt* chromitite, *Hx* harzburgite

in the G chromitites, whereas the orthopyroxene grains in the basal harzburgite and bronzitite have the lowest  $\delta^7\text{Li}$  values (Fig. 6a).

In contrast to Li isotopes, oxygen isotopic compositions are rather homogeneous in olivine, orthopyroxene and clinopyroxene. Regardless of the host lithology,



**Fig. 5** Chondrite-normalized rare earth element patterns of orthopyroxene (a, b) and clinopyroxene (c) in rocks from the Ultramafic Zone of the Stillwater Complex. Samples from the G chromitite zone are indicated in dashed lines, and samples from the lowermost layer in solid lines. Chondrite normalizing values are from Anders and Grevesse (1989)

olivine has limited  $\delta^{18}\text{O}$  variation from 4.91 to 5.72‰ (except for one analysis of 4.45‰), overlapping the  $\delta^{18}\text{O}$  values of clinopyroxene (4.64–5.86‰) and orthopyroxene (5.11–5.87‰) (Table 1), slightly lower than the values of orthopyroxene (5.7, 5.9 and 6.4‰) in mafic rocks of the Stillwater Complex (Dunn 1986) (Fig. 6b).

For convenience in the following discussion, Cr isotopic compositions reported in Bai et al. (2019) are also illustrated in Fig. 6c. Except for the basal harzburgite sample 16SW3-11 which has similar  $\delta^{53}\text{Cr}$  values in all its minerals, all the analyzed samples exhibit significant isotope fractionation between chromite and silicates. Olivine has higher  $\delta^{53}\text{Cr}$  values and larger variations than coexisting orthopyroxene, whereas  $\delta^{53}\text{Cr}$  values in chromite are uniform within analytical uncertainty (Bai et al. 2019).

## Discussion

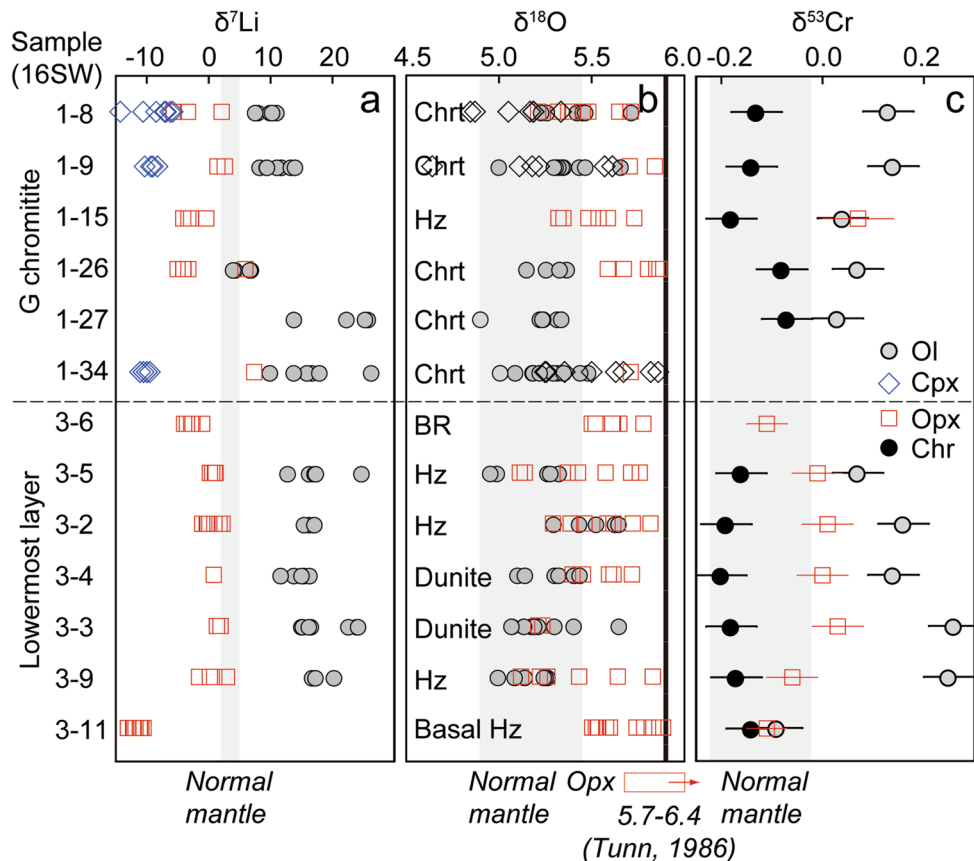
The minerals in the Ultramafic Zone of the Stillwater Complex show significant variations in Li and O isotopes and major and trace element compositions, which are comparable to the data reported in previous studies of the same complex and the Bushveld Complex. Experimental and empirical Li partition coefficients between silicate minerals have been well established e.g.,  $D_{\text{Li}} = 0.7$  (Brenan et al. 1998) and 0.8 (Eggins et al. 1998) for orthopyroxene/clinopyroxene, and  $D_{\text{Li}} = 1.3$  (Brenan et al. 1998) and 1.1–1.3 (Eggins et al. 1998) for olivine/clinopyroxene at temperature range of 800–1400 °C. The relative contents of Li between the different mineral phases from the Stillwater Complex are variable with  $^{O\text{I}/O\text{PxD}}$  ( $\text{Li}_{O\text{I}}/\text{Li}_{O\text{PxD}}$ ) values of 0.6–1.1 in the lowermost layer and 1.9–7.6 in the G chromitite and  $^{O\text{I}/C\text{PxD}}$  ( $\text{Li}_{O\text{I}}/\text{Li}_{C\text{PxD}}$ ) of 0.4–0.6 (Supplementary Table S3). They all do not match the above equilibrium values. The  $\Delta^7\text{Li}_{O\text{I}-O\text{PxD}}$  ( $\delta^7\text{Li}_{O\text{I}} - \delta^7\text{Li}_{O\text{PxD}} = 7.7\text{--}18.2$ ) and  $\Delta^7\text{Li}_{O\text{I}-C\text{PxD}}$  ( $\delta^7\text{Li}_{O\text{I}} - \delta^7\text{Li}_{C\text{PxD}} = 18.0\text{--}27.2$ ) values (Supplementary Table S3) range well beyond those expected for equilibration at high temperatures (–5 to 4‰; Rudnick and Ionov 2007). The inter-mineral Li elemental and isotopic disequilibria, as well as Cr isotopic disequilibrium (Fig. 6c; Bai et al. 2019), could be caused by subsolidus element exchange, magma differentiation and various reactions with melts/fluids. In the following subsections, we first constrain effects of subsolidus element exchange and crustal contamination on isotopic compositions of minerals, and then summarize the genetic connection between chemical compositions and variations in mineral assemblages and crystal sizes and magma differentiation control. We finally discuss the possible reactions to account for the inter-mineral and inter-sample mineralogical and geochemical variations.

### Effects of subsolidus element exchange on disequilibrated isotopic fractionations between minerals

The subsolidus element exchange between minerals is presumably extensive in the long cooling history of large layered intrusions (McCallum 2002; Schulte et al. 2010), and its effects on minerals depend on their composition and modal proportion (Jackson 1969; Xiao et al. 2016). Theoretically, the primary compositions of silicates are retained in silicate rocks whereas the silicates in chromitite have undergone extensive subsolidus exchange with chromite (Irvine 1967; Mondal et al. 2006; Mukherjee et al. 2010). In chromitites, olivine and pyroxenes reach their maximum Mg#s and Ni contents and their minimum Mn, Co and Ti



**Fig. 6** Li–O–Cr isotopic compositions of minerals in the stratigraphic section of the Ultramafic Zone of the Stillwater Complex. Oxygen isotopic compositions of orthopyroxene in peridotites of the Ultramafic Zone of the Stillwater Complex from Dunn (1986) are also plotted for comparison. The Cr isotopic data are from Bai et al. (2019). Normal mantle ranges of  $\delta^7\text{Li}$  (2.0–5.0‰),  $\delta^{18}\text{O}$  (4.90–5.46‰) and  $\delta^{53}\text{Cr}$  (–0.22 to –0.02‰) are from Elliott et al. (2006), Matthey et al. (1994), and Schoenberg et al. (2008), respectively. The bold black line in (b) represents a calculated  $\delta^{18}\text{O}$  value of 5.9‰ for the parental magma of the Stillwater Complex (Dunn 1986)



contents (Fig. 4), whereas the reverse compositions were observed in the associated chromite (Campbell and Murck 1993; Schulte et al. 2010). This is consistent with chemical exchange between silicate and chromite because elements such as Mg and Ni in chromite are relatively incompatible compared to Fe, Mn, Co, and Ti (Su et al. 2019).

Likewise, Cr is a major component in chromite but is typically present only as a trace to minor element in olivine and pyroxenes. Its diffusion from silicates to chromite should lead to negligible fractionation of Cr isotopes in chromite but significant fractionation in silicates, particularly for those in chromitites. This prediction, however, contradicts the measured inter-mineral  $\delta^{53}\text{Cr}$  fractionations of silicate rocks > chromitites (Fig. 6c; Bai et al. 2019). Moreover, in our basal harzburgite and bronzitite samples, identical  $\delta^{53}\text{Cr}$  values in orthopyroxene and olivine to chromite (Fig. 6) cannot be attributed to subsolidus element exchange between them.

The presence of orthopyroxene between olivine and chromite implies that in subsolidus exchange between olivine and chromite, if occurred, would have been impeded by the orthopyroxene mantles around the olivine grains. Because there are extremely low Li contents in chromite (Su et al. 2016, 2018), the occurrence of Li in olivine would reflect isotopic exchange between orthopyroxene

and olivine. Because of higher partition coefficient of Li in olivine than in orthopyroxene (Seitz and Woodland 2000), Li is expected to diffuse from orthopyroxene to olivine, resulting in Li depletion and  $\delta^7\text{Li}$  elevation in orthopyroxene and the reverse in olivine as  $^6\text{Li}$  diffuses faster than  $^7\text{Li}$  (Richter et al. 2003). It is, however, opposite to the obtained data (Figs. 7a, b, 8a, b), particularly, in some of our samples olivine has more variable and higher  $\delta^7\text{Li}$  values than orthopyroxene (Fig. 6a), although Li contents and  $\delta^7\text{Li}$  values of olivine plot along the modeling results of diffusion process (Fig. 7a). The relationship can apply to compositional variations between poikilitic clinopyroxene and olivine (Figs. 3o–s, 7c, 8c). Most olivine grains exhibit Li enrichment and  $\delta^7\text{Li}$  depletion in their rims relative to their cores (Fig. 9), consistent with expected trends of ingressive diffusion. However, Li contents and  $\delta^7\text{Li}$  values of orthopyroxene and clinopyroxene in similar rim-core profiles (Fig. 9) and their distributions in the entire dataset are totally inconsistent with experimental diffusion trends (Fig. 7b, c). Therefore, the compositional variations of the minerals in the Ultramafic Zone of the Stillwater Complex cannot be explained solely by subsolidus element exchange, and complex  $\delta^7\text{Li}$  profiles in olivine grains at inter- and intra-sample scales suggest additional processes to account for their compositional characteristics.

**Table 1** Li and O isotopes of olivine (Ol), orthopyroxene (Opx) and clinopyroxene (Cpx) in the rocks from the Ultramafic Zone of the Stillwater Complex

Sample	Rock type	Mineral	Grain@no	Comment	$\delta^{18}\text{O}$	2se	Li	1se	$\delta^7\text{Li}$	1se
16SW3-3	Dunite	Ol	1@1		5.18	0.23				
			2@1		5.22	0.20				
			3@1	Rim	5.20	0.35	1.96	0.01	24.16	0.51
			3@2		5.14	0.19	1.97	0.01	24.10	0.56
			3@3		5.31	0.25	1.88	0.01	22.74	0.64
			3@4	Core	5.41	0.22	1.62	0.01	24.33	0.63
			4@1	Rim	5.08	0.27	2.46	0.01	15.14	0.51
			4@2		5.14	0.19	2.50	0.01	15.38	0.60
			4@3		5.07	0.23	2.47	0.01	16.71	0.52
			4@4	Core	5.65	0.18	2.42	0.01	16.35	0.78
16SW3-4	Dunite	Ol	1@1	Rim	5.11	0.20	2.39	0.01	13.96	0.58
			1@2		5.31	0.22	2.20	0.01	15.52	0.57
			1@3		5.33	0.17	2.08	0.01	16.47	0.54
			1@4	Core	5.41	0.17	2.16	0.01	15.19	0.52
			2@1		5.41	0.18				
			3@1		5.15	0.24				
			4@1		5.44	0.26	2.28	0.01	11.81	0.60
16SW3-2	Harzburgite	Ol	1@1	Rim	5.30	0.18	3.47	0.01	17.14	0.40
			1@2		5.53	0.26	3.21	0.01	16.42	0.50
			1@3		5.63	0.14	3.07	0.01	15.59	0.48
			1@4	Core	5.65	0.18	2.90	0.01	17.26	0.49
			2@1		5.44	0.10				
16SW3-9	Harzburgite	Ol	1@1		5.00	0.18				
			2@1	Rim	5.27	0.20	2.60	0.01	17.01	0.51
			2@2		5.26	0.27	2.43	0.01	20.43	0.41
			2@3		5.25	0.33	2.34	0.01	16.89	0.44
			2@4	Core	5.15	0.25	2.27	0.01	17.44	0.55
			3@1		5.09	0.15				
16SW3-5	Harzburgite	Ol	1@1	Rim	5.27	0.24	2.62	0.01	16.40	0.47
			1@2		4.99	0.25	2.39	0.01	12.93	0.54
			1@3		5.33	0.23	2.34	0.01	17.29	0.50
			1@4	Core	4.96	0.18	2.36	0.01	17.50	0.54
			2@1		5.28	0.12				
			3@1		4.45	0.56	1.42	0.00	24.87	0.54
16SW1-8	Disseminated chromitite	Ol	1@1		5.27	0.19				
			2@1	Rim	5.43	0.31	3.15	0.01	8.10	0.44
			2@2		5.46	0.36	2.98	0.01	11.12	0.50
			2@3		5.47	0.26	3.12	0.01	10.14	0.50
			2@4	Core	5.23	0.22	3.19	0.01	7.71	0.42
			3@1		5.72	0.20	2.84	0.01	10.43	0.46
16SW1-9	Disseminated chromitite	Ol	1@1		5.44	0.22				
			2@1	Rim	5.66	0.12	2.84	0.01	8.41	0.38
			2@2		5.35	0.31	2.76	0.01	11.84	0.46
			2@3	Core	5.35	0.19	2.47	0.01	11.92	0.55
			3@1	Rim	5.47	0.16	2.93	0.01	9.55	0.38
			3@2		5.01	0.28	2.90	0.01	11.22	0.52
			3@3		5.33	0.19	2.76	0.01	9.61	0.50
			3@4		5.31	0.19	2.04	0.01	13.48	0.63
			3@5	Core	5.30	0.21	1.92	0.01	14.13	0.56

**Table 1** (continued)

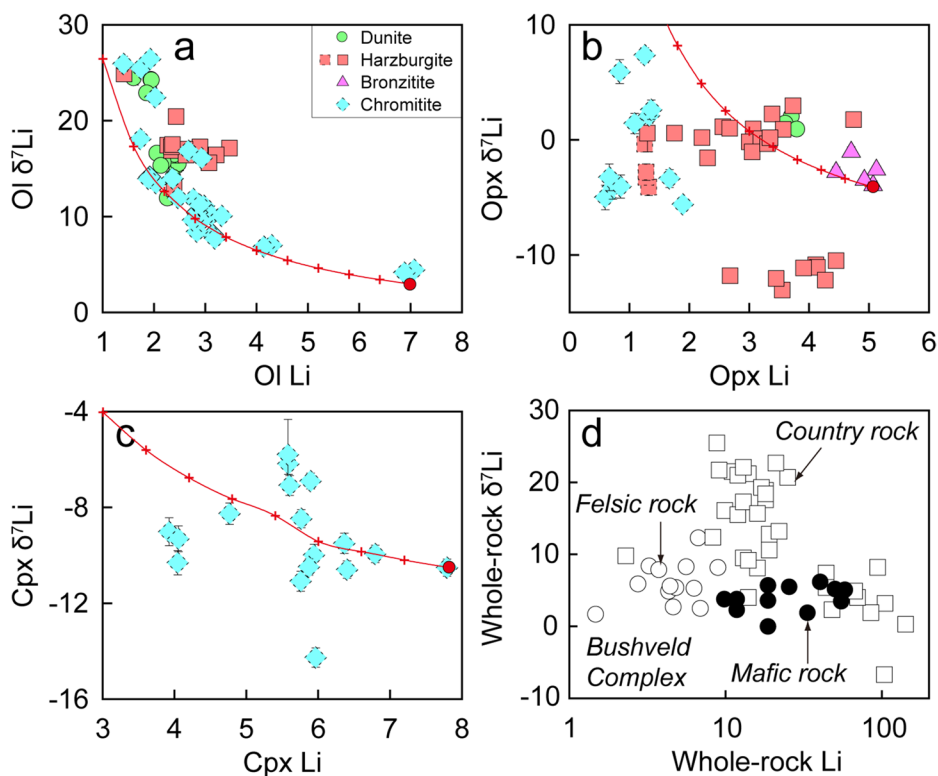
Sample	Rock type	Mineral	Grain@no	Comment	$\delta^{18}\text{O}$	2se	Li	1se	$\delta^7\text{Li}$	1se
16SW1-26	Disseminated chromitite	Ol	1@1	Rim	5.37	0.14	7.07	0.02	4.45	0.33
			1@2		5.26	0.19	6.88	0.03	4.14	0.29
			1@3		5.33	0.18	4.29	0.01	7.00	0.45
			1@4	Core	5.15	0.20	4.14	0.01	6.85	0.46
16SW1-27	Disseminated chromitite	Ol	1@1		5.23	0.19				
			2@1		5.32	0.32				
			3@1	Rim	4.91	0.22	1.41	0.01	25.91	0.80
			3@2		5.25	0.21	1.74	0.01	25.45	0.72
			3@3		5.34	0.34	2.03	0.01	22.44	0.62
			3@4	Core	5.24	0.26	2.36	0.01	13.97	0.53
16SW1-34	Disseminated chromitite	Ol	1@1	Rim	5.49	0.26	2.67	0.01	16.84	0.47
			1@2		5.09	0.20				
			1@3		5.01	0.22				
			1@4	Core	5.19	0.17	2.93	0.01	16.08	0.46
			2@1		5.32	0.24	3.32	0.01	10.07	0.43
			3@1		5.30	0.17				
			4@1		5.19	0.20	1.93	0.00	26.43	0.59
			5@1	Rim	5.44	0.16				
			5@2	Core	5.36	0.20	1.73	0.01	18.08	0.74
			5@3		5.23	0.27	1.89	0.01	13.93	0.56
16SW3-3	Dunite	Opx	1@1		5.23	0.25	3.72	0.01	1.93	0.45
			2@1		5.21	0.20	3.62	0.01	1.33	0.51
16SW3-4	Dunite	Opx	1@1		5.72	0.27	3.81	0.03	0.81	0.39
			2@1	Rim	5.45	0.23				
			2@2		5.59	0.19				
			2@3		5.40	0.18				
			2@4	Core	5.62	0.19				
16SW3-2	Harzburgite	Opx	1@1	Rim	5.62	0.12	3.07	0.01	0.94	0.50
			1@2		5.59	0.18	3.00	0.01	-0.19	0.48
			1@3		5.82	0.13	3.19	0.01	0.10	0.48
			1@4	Core	5.29	0.22	3.05	0.01	-1.05	0.49
			2@1		5.72	0.28	3.38	0.02	2.24	0.46
			3@1		5.46	0.28	3.30	0.02	-0.34	0.53
			4@1		5.39	0.19	4.74	0.01	1.76	0.42
16SW3-9	Harzburgite	Opx	1@1		5.26	0.22	2.31	0.01	-1.57	0.63
			2@1	Rim	5.64	0.23	3.73	0.01	2.96	0.57
			2@2		5.43	0.17				
			2@3		5.22	0.30				
			2@4	Core	5.83	0.12	3.57	0.01	0.91	0.43
			3@1		5.12	0.38	3.35	0.01	0.18	0.48
16SW1-15	Harzburgite	Opx	1@1	Rim	5.54	0.20	1.32	0.01	-4.10	0.74
			1@2		5.32	0.26	1.27	0.00	-3.27	0.64
			1@3		5.35	0.20	1.28	0.00	-2.80	0.72
			1@4	Core	5.73	0.29	1.25	0.00	-0.38	0.68
			2@1		5.59	0.20				
			3@1		5.48	0.24				
16SW3-5	Harzburgite	Opx	1@1		5.58	0.25				
			2@1		5.37	0.26				
			3@1	Rim	5.14	0.22	1.30	0.01	0.58	1.61
			3@2		5.43	0.30	1.75	0.01	0.57	0.64

Table 1 (continued)

Sample	Rock type	Mineral	Grain@no	Comment	$\delta^{18}\text{O}$	2se	Li	1se	$\delta^7\text{Li}$	1se
16SW3-11	Basal Pl-harzburgite	Opx	3@3		5.76	0.25	2.21	0.01	0.20	0.53
			3@4		5.71	0.25	2.56	0.01	1.13	0.63
			3@5	Core	5.11	0.22	2.67	0.01	1.01	0.50
			1@1		5.60	0.27				
			2@1	Rim	5.53	0.18	2.68	0.01	-11.81	0.64
			2@2	Core	5.52	0.21	3.55	0.01	-13.05	0.47
			3@1		5.89	0.23	3.45	0.01	-12.06	0.45
			4@1		5.74	0.18	4.45	0.02	-10.51	0.48
			5@1		5.78	0.29				
			6@1	Rim	5.83	0.28	4.11	0.01	-10.87	0.44
16SW3-6	Orthopyroxenite	Opx	6@2		5.58	0.20	4.14	0.01	-11.08	0.41
			6@3		5.50	0.28	3.91	0.01	-11.13	0.42
			6@4	Core	5.54	0.28	4.27	0.01	-12.21	0.50
			1@1		5.50	0.19				
			2@1		5.59	0.27				
			3@1	Rim	5.65	0.14	5.07	0.01	-3.97	0.41
			3@2		5.61	0.17	5.13	0.01	-2.61	0.35
			3@3		5.52	0.24	4.92	0.01	-3.50	0.41
			3@4		5.61	0.26	4.70	0.02	-1.05	0.44
			3@5	Core	5.78	0.28	4.45	0.01	-2.81	0.46
16SW1-8	Disseminated chromitite	Opx	1@1		5.71	0.27	1.33	0.00	2.10	0.68
			2@1		5.37	0.21	1.67	0.01	-3.36	0.77
			3@1		5.65	0.23	1.89	0.00	-5.61	0.52
			4@1	Rim	5.45	0.29				
			4@2		5.21	0.17				
			4@3		5.40	0.23				
			4@4		5.32	0.21				
			4@5	Core	5.48	0.23				
16SW1-9	Disseminated chromitite	Opx	1@1		5.84	0.15	1.36	0.00	2.61	0.84
			2@1		5.71	0.21	1.09	0.01	1.41	0.88
16SW1-26	Disseminated chromitite	Opx	1@1	Rim	5.59	0.33	0.60	0.00	-5.01	1.07
			1@2	Core	5.85	0.15	0.84	0.00	5.92	1.03
			2@1		5.67	0.26	0.72	0.00	-4.09	1.08
			3@1		5.80	0.23	0.85	0.00	-4.06	1.01
			4@1		5.87	0.21	0.66	0.00	-3.27	1.16
16SW1-34	Disseminated chromitite	Opx	1@1		5.71	0.18	1.25	0.00	7.35	0.66
16SW1-8	Disseminated chromitite	Cpx	1@1	Rim	5.19	0.30	5.58	0.01	-6.19	0.43
			1@2		5.17	0.25	5.76	0.01	-8.47	0.38
			1@3		5.05	0.19	5.58	0.01	-5.81	1.47
			1@4		4.87	0.17	5.60	0.01	-7.09	0.42
			1@5	Core	4.85	0.23	5.89	0.01	-6.90	0.33
			2@1		5.33	0.30	5.97	0.01	-14.27	0.40
			3@1		5.19	0.25	6.40	0.02	-10.60	0.36
			1@1		5.57	0.34				
16SW1-9	Disseminated chromitite	Cpx	2@1	Rim	5.22	0.17	3.93	0.01	-9.02	0.58
			2@2		4.64	0.25	4.05	0.01	-10.32	0.51
			2@3		5.11	0.33	4.77	0.01	-8.27	0.44
			2@4	Core	5.18	0.13	4.06	0.01	-9.32	0.54
			3@1		5.61	0.26				
16SW1-34	Disseminated chromitite	Cpx	1@1	Rim	5.25	0.42				

**Table 1** (continued)

Sample	Rock type	Mineral	Grain@no	Comment	$\delta^{18}\text{O}$	2se	Li	1se	$\delta^7\text{Li}$	1se
			1@2	Core	5.50	0.22				
			2@1	Rim	5.67	0.20	5.94	0.01	-9.99	0.45
			2@2		5.86	0.33	5.76	0.01	-11.08	0.42
			2@3		5.35	0.22	5.87	0.01	-10.49	0.34
			2@4	Core	5.26	0.23	6.36	0.04	-9.50	0.42
			3@1	Rim	5.82	0.23	6.79	0.01	-9.94	0.36
			3@2	Core	5.63	0.26	7.79	0.02	-10.52	0.36



**Fig. 7** Correlation diagrams of Li and  $\delta^7\text{Li}$  for olivine (a), orthopyroxene (b) and clinopyroxene (c) in rocks from the Ultramafic Zone of the Stillwater Complex, with comparison of data from the Bushveld Complex (Ireland and Penniston-Dorland 2015) (d). Red solid line with stars in (a–c) is the modeling result of Li diffusion between solid phases and interstitial liquid using a Rayleigh distillation process. Initial compositions of olivine are assumed as 7 ppm Li and 3.0‰  $\delta^7\text{Li}$ , and the compositions of the interstitial liquid are the mean values of orthopyroxene (Li=3 ppm;  $\delta^7\text{Li}=-2.0\text{‰}$ ). Initial

compositions of orthopyroxene are assumed as 5 ppm Li and  $-4.0\text{‰}$   $\delta^7\text{Li}$  of the Li-richest analysis, and the compositions of the interstitial liquid are 4 ppm Li and  $-11.6\text{‰}$   $\delta^7\text{Li}$  of the  $\delta^7\text{Li}$ -lowest analysis. Initial compositions of clinopyroxene are assumed as 7.8 ppm Li and  $-10.5\text{‰}$   $\delta^7\text{Li}$  of the Li-richest analysis, and the compositions of the interstitial liquid are 6 ppm Li and  $-14.3\text{‰}$   $\delta^7\text{Li}$  of the  $\delta^7\text{Li}$ -lowest analysis. Samples from the G chromitite zone are indicated in dashed symbols, and samples from the lowermost layer in solid symbols

### Effects of crustal contamination on mineral Li and O isotopic compositions

The properties of Li, a moderately incompatible and fluid-mobile element with a mass difference of  $\sim 17\%$  between the two stable isotopes ( $^6\text{Li}$  and  $^7\text{Li}$ ), make it a useful tracer for various melt/fluid–rock interactions (Chan et al. 1992; Su

et al. 2014, 2018). Crustal contamination in mantle-derived magmas can be identified by Li isotope systematics, because crustal rocks typically have higher Li concentrations (several to hundreds ppm) and more variable but overall higher  $\delta^7\text{Li}$  values than mantle rocks (Tomascak et al. 2016). Studies of the Bushveld Complex revealed that involvement of country rocks resulted in significant elevation of Li concentrations

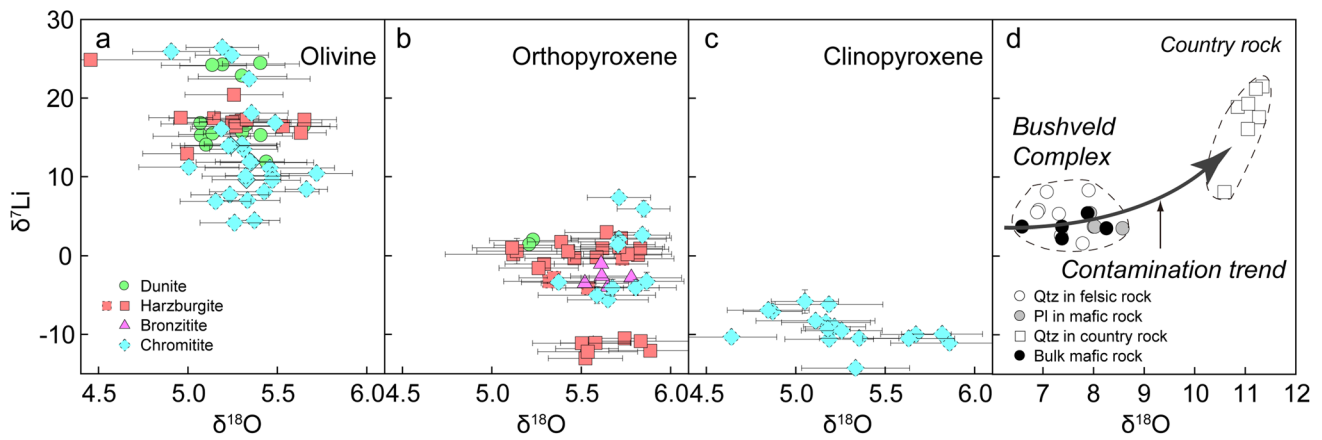


**Fig. 8** Correlation diagrams of  $\delta^{18}\text{O}$  and  $\delta^7\text{Li}$  for olivine (a), orthopyroxene (b) and clinopyroxene (c) in rocks from the Ultramafic Zone of the Stillwater Complex, with comparison of data from the Bush-

veld Complex (Ireland and Penniston-Dorland 2015) (d). Samples from the G chromitite zone are indicated in dashed symbols, and samples from the lowermost layer in solid symbols

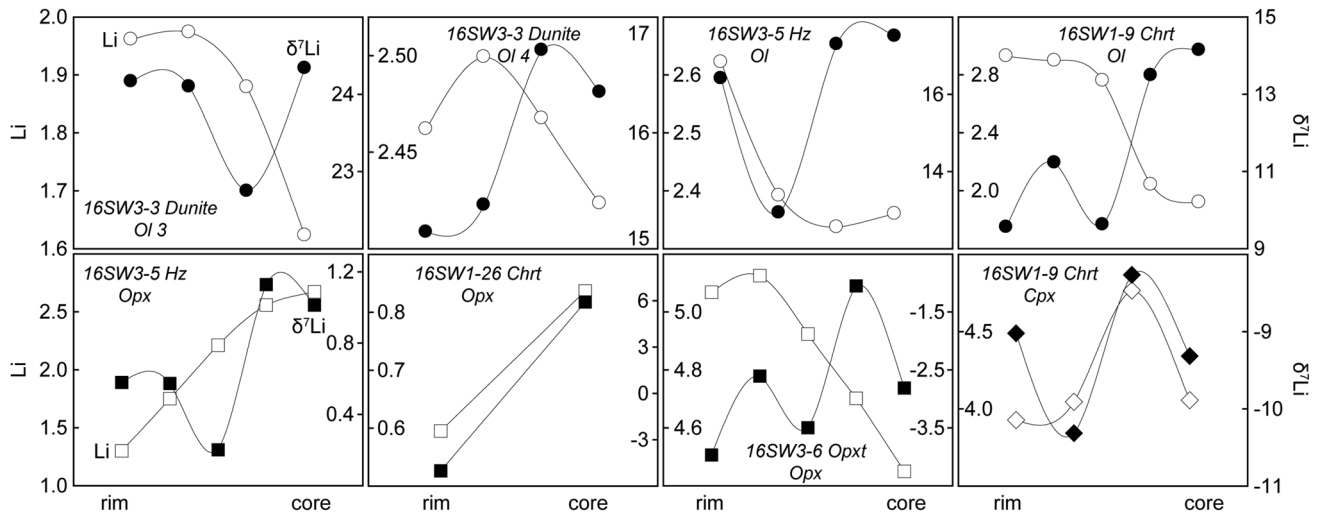


**Fig. 9** Representative rim-core profile analyses of Li elemental and isotopic compositions of mineral grains in rocks from the Ultramafic Zone of the Stillwater Complex

in mafic rocks ( $\text{Li} > 10$  ppm) and felsic ones ( $\text{Li} < 10$  ppm) but only slight  $\delta^7\text{Li}$  variations in bulk rock samples (Fig. 7d) (Ireland and Penniston-Dorland 2015). Since olivine and pyroxene are the major hosts of Li in the studied rocks from the Stillwater Complex, their  $< 7$  ppm Li concentrations and large  $\delta^7\text{Li}$  variations (Fig. 7a–c) could approximately represent whole-rock compositions and are apparently inconsistent with indicators of contamination in the Bushveld Complex. The negative correlation between Li and  $\delta^7\text{Li}$  in the olivine (Fig. 7a) and the lack of their correlations in either orthopyroxene or clinopyroxene (Fig. 7b, c) in the Stillwater Complex suggest insignificant effects of crustal contamination on their Li isotope systematics.

Previous studies of O isotopes of the Stillwater Complex revealed that the intrusion has retained its magmatic isotopic

composition with a calculated  $\delta^{18}\text{O}$  value of 5.9‰ (Dunn 1986), agreeing well with mantle-derived melts ( $\sim 5.7$ ‰, Eiler 2001). These values show that most of the isotopic variations within the complex can be accounted for by simple fractional crystallization (Dunn, 1986). The  $\delta^{18}\text{O}$  ranges of both olivine and pyroxenes in the Ultramafic Zone of the complex are between normal mantle values and those estimated for the entire complex (Fig. 6b), indicating negligible effects of crustal contamination on O isotope systematics. The O isotopic compositions of these minerals do not co-vary with  $\delta^7\text{Li}$  values (Fig. 8a–c), which is inconsistent with the contamination trend defined from the studies of the Bushveld Complex (Fig. 8d; Ireland and Penniston-Dorland 2015). Hence, crustal contamination, if it occurred, did not significantly modify the Li and O isotopic compositions of

the parental magma of the Stillwater Complex. In addition, large inter-sample  $\delta^7\text{Li}$  and intra- and inter-sample  $\delta^{18}\text{O}$  variations of orthopyroxene and clinopyroxene cannot be explained by incongruent melting, which would not produce Li and O isotopic fractionation but significant Li depletion.

### **Links between mineral composition, mineral assemblage and crystal size, and controls of magma differentiation**

Compositionally, there are no observable variations in terms of element concentrations and Li and O isotopes in olivine from the Stillwater harzburgites and dunites, but abrupt changes, particularly in Mg#, transition metal element contents, and Li and Cr isotopes, are obvious between silicate rocks and chromitite seams (Figs. 4, 6), probably related to cooling and re-equilibration between minerals and/or interstitial liquids. Correspondingly, in transitions from chromitite and dunite to poikilitic harzburgite and bronzitite chromite and olivine abundances generally show gradually decreasing trends whereas orthopyroxene, clinopyroxene and plagioclase increase. The average chromite crystal size increases uniformly upward from the base within an individual cyclic unit (Fig. 3g; Boudreau 2011), but then decreases abruptly directly above the chromitite seam. From there it increases monotonically to the top of the unit (Figs. 2a–c, 3; Cooper 1990). In general, increases in olivine crystal size are most conspicuous in poikilitic harzburgites and some dunites (Fig. 3b–e; Boudreau 2011). These links between mineral assemblage, crystal size and chemical composition are also compatible to field observations (Fig. 2a, d). A regular decrease in the size and abundance of orthopyroxene oikocrysts in olivine-rich rocks occurs near gradational contacts or, more rarely, sharp contacts between dunite and poikilitic harzburgite over a meter scale (Jones et al. 1960; Jackson 1961; Jenkins and Mungall 2018). The sharp physical contact and the abrupt chemical changes have been related to breaks in injection of magma into the chamber (Jackson 1970) or truncation of the previous cyclic unit by a low-angle magmatic unconformity (Cooper 1997). Both explanations imply distinct parental magmas or various post-cumulus modifications for chromitites and silicate rocks or abrupt compositional changes of a single magma pulse during formation of an individual unit.

The inter-lithological compositional differences might also be controlled by crystallization sequence and the spatial relations of minerals. This inference is supported by a lack of negative Eu anomalies and slight LREE enrichment in orthopyroxene and clinopyroxene in some chromitite samples (e.g., 16SW1-8; Fig. 5b, c) in which plagioclase is absent, because plagioclase normally accommodates large amounts of LREE and Eu (Lambert and Simmons 1987). Consequently, REE patterns of orthopyroxene in harzburgite

and bronzitite (Fig. 5a) suggest that these rocks formed from an evolved magma which had previously experienced plagioclase fractionation. In a few chromitite samples LREE depletion and Eu anomalies of their pyroxenes (Fig. 5b, c; Lambert and Simmons 1987) suggest that the parental magmas of these chromitites experienced concurrent crystallization of plagioclase (McCallum 1996) or mixing with an evolved magma.

Isotopically, the generally decreasing trend of  $\delta^7\text{Li}$  values (and the increasing trend of Li contents in the lowermost layer) from olivine to orthopyroxene and clinopyroxene (Fig. 8a–c) is consistent with magma differentiation, which normally results in Li increasing and  $^6\text{Li}$  enrichment in evolving melts (Su et al. 2017), and further confirms the crystallization order of these coexisting minerals. The Li content and  $\delta^7\text{Li}$  co-variations in rim-core profile analyses of orthopyroxene and clinopyroxene (Fig. 9) reveal their growth from evolving magmas. Taking into account inter-sample variations,  $\delta^7\text{Li}$  values in olivine, although negatively correlated with Li concentrations as a whole, show larger variations in chromitite than in silicate rocks (Fig. 7a). This indicates formation from distinct parental magmas or various post-cumulus modifications. Moreover, the absence of correlations between Li and  $\delta^7\text{Li}$  in orthopyroxene and clinopyroxene (Fig. 7b, c) is compatible with crystallization from different parental magmas.

### **Formation of poikilitic pyroxenes**

The above discrepancies are closely related to the formation of orthopyroxene and clinopyroxene oikocrysts in large layered intrusions. The formation of poikilitic textures is dependent on differences in the nucleation rate and/or the growth rate of the different minerals; oikocrysts form if one mineral has a lower nucleation rate but higher growth rate than co-accumulating crystals of another phase (Kaufmann et al. 2018). Three main hypotheses have been proposed: (1) Oikocrysts form in the post-cumulus stage by solidification of interstitial liquid (e.g., Wager et al. 1960); (2) they are cotectic grains lacking compositional zonation but having compositions typical of primocrysts of the same phase (Barnes et al. 2016). (3) Pyroxene oikocrysts form by reactive replacement of olivine primocrysts by upward-percolating melts, followed by poikilitic overgrowth of oikocryst cores from a more primitive melt (Kaufmann et al. 2018).

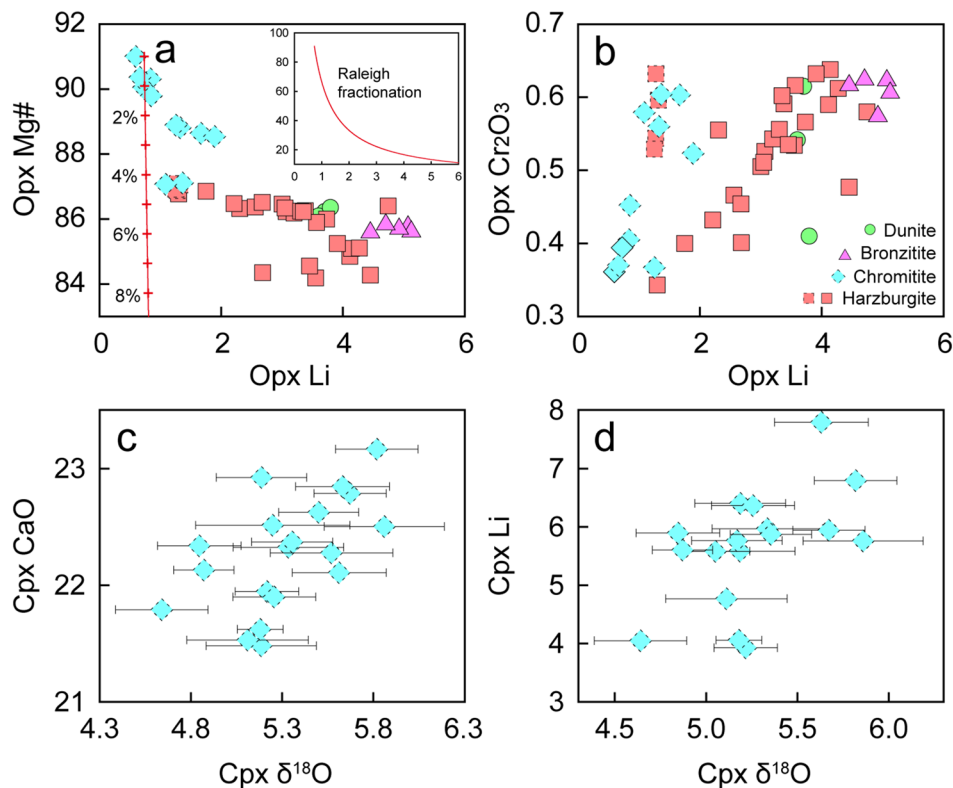
The occurrence and morphological features of chromite and olivine in ultramafic rocks show that they are cumulus phases (Fig. 3b–s; Jackson 1961; McCallum 1996; Cooper 1997). The nature of contacts between chromite and olivine through orthopyroxene or clinopyroxene does not always fit the classic cumulus model. For example, most chromite grains in the Ultramafic Zone are surrounded by pyroxenes and the abundance of chromite in different sections varies.

Where chromite is concentrated in thin and massive layers, the interstitial mineral is largely orthopyroxene, whereas where chromite is less abundant, olivine is more abundant (Howland et al. 1949). These characteristics suggest that chromite and olivine did not crystallize simultaneously in cotectic proportions, rather the chromite grains appear to have been transported by liquids, from which the pyroxenes crystallized, and were then emplaced within cumulus olivine piles. The intrusion of chromite-rich liquids physiochemically modified the olivine grains before their complete solidification. The olivine crystals were smoothed to round shapes (Fig. 3b–s), and the presence of tiny olivine remnants in pyroxene (Fig. 3m) indicates reaction replacement. The reaction should have been less extensive than that observed in the Bushveld complex, where orthopyroxene oikocrysts are larger but contain fewer remnants of olivine (Kaufmann et al. 2018). The narrow variation of intra-grain Li isotopic compositions (Figs. 6a, 9) and the absence of a negative correlation between  $\delta^7\text{Li}$  and Li abundance (Fig. 7b, c) in the pyroxenes reflect no significant elemental diffusion after crystallization. We thus conclude that poikilitic pyroxenes formed from a chromite-saturated liquid, which added an external component to cumulus olivine piles and resulted in replacive reaction of the olivine.

The compositions of pyroxene crystallized from chromite-rich magma would depend on competition for elements posed by the co-precipitating chromite. The most intense

competitions will be for Fe, Cr, Al, and Mg rather than Ca, Li and O owing to their contrasting partition coefficients between chromite and pyroxenes (Schulte et al. 2010). As a consequence, in a given cycle in the Stillwater Complex from chromitite through harzburgite to bronzitite, orthopyroxenes show significant Li increases with only small changes in Mg# (Fig. 10a), whereas a generally positive correlation between Li and  $\text{Cr}_2\text{O}_3$  (Fig. 10b) reflects decreasing competition for Cr due to lower chromite crystallization. These relationships are further supported by positive correlations between  $\delta^{18}\text{O}$  values and CaO and Li concentrations in the clinopyroxene (Fig. 10c, d). Similarly, because chromite structurally contains very minor or no REE, its crystallization would have negligible effect on the overall REE abundance. The increasing enrichment of LREE in orthopyroxene from chromitite to bronzitite (Fig. 5a, b) reflects a trend of fractional crystallization or compositional change of the parental magma. The Li isotopic compositions of the orthopyroxene are homogeneous in individual samples but are heterogeneous on a larger scale (Fig. 6a), further suggesting that the melts, from which orthopyroxene crystallized, had locally uniform  $\delta^7\text{Li}$  values but highly varying within the magma chamber. Compositional changes in the melts were likely due to mixing between fractionated magma and newly injected primitive melts because the variations in  $\delta^{18}\text{O}$  of the orthopyroxene fluctuate between normal mantle values and those of the estimated parental magma of the

**Fig. 10** Correlation diagrams of Li vs. Mg# (a) and  $\text{Cr}_2\text{O}_3$  (b) for orthopyroxene and  $\delta^{18}\text{O}$  vs. CaO (c) and Li (d) for clinopyroxene in rocks from the Ultramafic Zone of the Stillwater Complex. Raleigh fractionation calculation shown in a indicates that orthopyroxene crystallized from compositionally varying melts. Samples from the G chromitite zone are indicated in dashed symbols, and samples from the lowermost layer in solid symbols





Stillwater Complex (Fig. 6b). This inference receives further support from an apparent shift of the orthopyroxene data from Raleigh fractionation line (Fig. 10a).

### Reaction between interstitial liquids and cumulus minerals

Olivine grains in the Stillwater chromitites have larger compositional variations, particularly in terms of major and trace elements (Fig. 4) and Li, O and Cr isotopes (Figs. 6, 7a, 8a) than those in the silicate rocks. This indicates complex processes involved in the olivine formation. For a given sample, olivine displays more variable and higher  $\delta^7\text{Li}$  but lower  $\delta^{18}\text{O}$  values than orthopyroxene, indicating that olivine experienced more extensive post-crystallization compositional modification than the orthopyroxene. Modeling results assuming the highest-Li analysis as initial compositions of olivine and mean values of orthopyroxene as the compositions of interstitial liquid demonstrate that negative correlations between Li and  $\delta^7\text{Li}$  in olivine can be attributed to kinetic diffusion with interstitial liquid (Fig. 7a).

The observed positive correlation between  $\delta^7\text{Li}$  and  $\delta^{53}\text{Cr}$  values in olivine (Fig. 11a) would not have been generated by Cr diffusion from olivine to chromite (Xia et al. 2017; Bai et al. 2019). Instead, Cr isotopic changes of the reacting liquids due to chromite crystallization were more likely responsible for the  $\delta^{53}\text{Cr}$  variations in the olivine, which is evident from the positive correlation between chromite  $\delta^{53}\text{Cr}$

and olivine  $\delta^7\text{Li}$  (Fig. 11b). Constant  $\delta^{18}\text{O}$  values in olivine showing no correlation with either  $\delta^{53}\text{Cr}$  or  $\delta^7\text{Li}$  indicate no visible modification (Figs. 7a, 11c) in O isotopes in olivine during its reaction with the liquids, which were probably newly injected primitive magma (Raedeke and McCallum 1984; Campbell and Murck 1993; Lipin 1993; Cawthorn et al. 2005). The absence of co-variations between  $\delta^7\text{Li}$ ,  $\delta^{18}\text{O}$  and  $\delta^{53}\text{Cr}$  values in pyroxenes, chromite and olivine (Figs. 7b, c, 11d–f) further confirms the isotopic variations are related to the reacting liquid. Development of fractures and poorly-defined grain boundaries of some chromite grains enclosed within clinopyroxene (Fig. 3p–r) demonstrates physical as well as composition modification by the liquids. Low  $\delta^{18}\text{O}$  values (2.2 and 3.2‰) of chromite from the Stillwater Complex reported by Mondal et al. (2003) are consistent with high-temperature alteration.

The interstitial liquid, from which pyroxenes mainly crystallized, reacted with the olivine and significantly modified its chemical composition (Barnes 1986) (Fig. 6). Simultaneously the compositions of the interstitial liquid were also modified. As the chromite grains collected hydrous fluids on their crystal surfaces due to the wetting property of chromite (Matveev and Ballhaus 2002), chromite compaction would lead to expelling of the hydrous fluids and outward penetration or upward transportation (Su et al. 2020). Outward penetration yielded additional modification on olivine compositions and occasionally on chromite. The fluids are believed to have been the parent

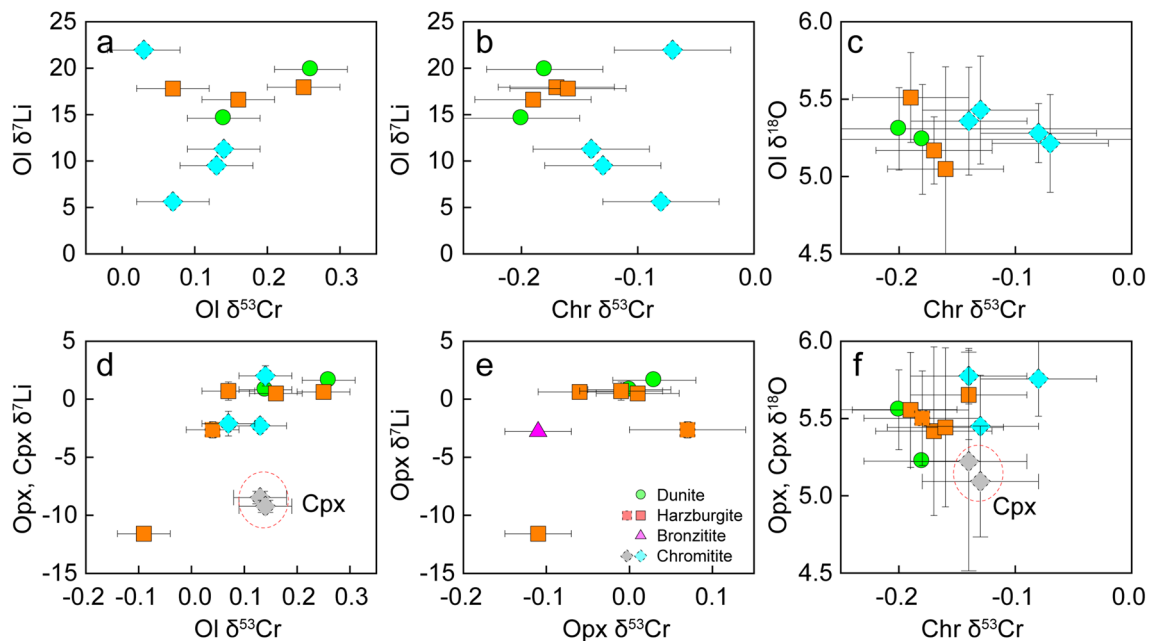


**Fig. 11** Multiple correlation diagrams of average  $\delta^{18}\text{O}$ , average  $\delta^7\text{Li}$  and  $\delta^{53}\text{Cr}$  values for minerals in rocks from the Ultramafic Zone of the Stillwater Complex. Clinopyroxene data are indicated in gray in

plots **d** and **f**. Samples from the G chromitite zone are indicated in dashed symbols, and samples from the lowermost layer in solid symbols

magma of clinopyroxene and some hydrous minerals in stratiform and podiform chromitites (McDonald 1965; Matveev and Ballhaus 2002; Boudreau 2016; Johan et al. 2017; Su et al. 2019, 2020), and, thus, they were likely sources of clinopyroxene crystals in chromite seams and pegmatites in the Stillwater Complex. During formation of the harzburgite and bronzitite layers, infiltration of upward ascending hydrous fluids from the chromite seams would have enhanced chemical exchange between cumulus minerals (Bai et al. 2019; Su et al. 2020). The evolved magma after separation from the ultramafic cumulates would have become a new starting point of a repeated process of magma mixing and subsequent formation of a new cyclic unit.

## Conclusion

Both olivine and pyroxenes in chromitite, dunite, poikilitic harzburgite and bronzitite from the Ultramafic Zone of the Stillwater Complex show large  $\delta^7\text{Li}$  variations and relatively homogeneous oxygen isotopic compositions. In individual samples, olivine has more variable and higher  $\delta^7\text{Li}$  values than pyroxenes, whereas  $\delta^{18}\text{O}$  values in olivine are basically within normal mantle ranges and lower than orthopyroxene. Clinopyroxene in the chromitites displays a narrow  $\delta^7\text{Li}$  range and the widest  $\delta^{18}\text{O}$  variations. The general Li and O isotopic compositions and inter-mineral and inter-sample isotopic variations are correlated with mineral assemblages, crystal sizes and major and trace element compositions, suggesting various reactions between interstitial liquids, from which pyroxenes crystallized, and the cumulus minerals. Integration of rare earth element patterns and Cr isotope variations indicates that compositional changes in the interstitial liquids were the main controlling factor, in addition to mineral fractionation and subsolidus chemical exchange, on the mineral compositions. Hydrous fluids collected on the surfaces of chromite grains provided a critical medium for extensive chemical exchange between chromite and olivine, and their release might have contributed to generation of hydrous minerals and pegmatites in the Stillwater Complex. Mixing between fractionated magma and a newly injected primitive melt can account for the compositional changes in the interstitial liquids.

**Acknowledgements** We appreciate the constructive reviews from Daniela Rubatto, Alan E. Boudreau and an anonymous reviewer, who markedly improved the paper. This study was supported by the National Natural Science Foundation of China (91755205 and 41772055) and the Second Tibetan Plateau Scientific Expedition and Research Program (STEP) (2019QZKK0801).

## References

- Aird HM, Ferguson KM, Lehrer ML, Boudreau AE (2017) A study of the trace sulfide mineral assemblages in the Stillwater Complex, Montana, USA. *Miner Deposita* 52:361–382
- Anders E, Grevesse N (1989) Abundances of the elements: meteoritic and solar. *Geochim Cosmochim Acta* 53:197–214
- Bai Y, Su BX, Xiao Y, Chen C, Cui MM, He XQ, Qin LP, Charlier B (2019) Diffusion-driven chromium isotope fractionation in minerals of ultramafic cumulates: elemental and isotopic evidence from the Stillwater Complex. *Geochim Cosmochim Acta* 263:167–181
- Barnes SJ (1986) The effect of trapped liquid crystallization on cumulus mineral compositions in layered intrusions. *Contrib Miner Petrol* 93:524–531
- Barnes SJ, Mole DR, Le Vaillant M, Campbell MJ, Verrall MR, Roberts MP, Evans NJ (2016) Poikilitic textures, heteradcumulates and zoned orthopyroxenes in the Ntaka ultramafic complex, Tanzania: implications for crystallization mechanisms of oikocrysts. *J Petrol* 57:1171–1198
- Brenan JM, Neroda E, Lindstrom CC, Shaw HF, Ryerson FJ, Phinney DL (1998) Behaviour of boron, beryllium and lithium during melting and crystallization: constraints from mineral-melt partitioning experiments. *Geochim Cosmochim Acta* 62:2129–2141
- Boudreau AE (2011) The evolution of texture and layering in layered intrusions. *Intern Geol Rev* 53:330–353
- Boudreau AE (2016) The Stillwater Complex, Montana—overview and the significance of volatiles. *Mineral Mag* 80:585–637
- Campbell IH, Murck BW (1993) Petrology of the G and H chromitite zones in the Mountain View area of the Stillwater Complex, Montana. *J Petrol* 34:291–316
- Cawthorn RG, Barnes SJ, Ballhaus C, Malitch KN (2005) Platinum-group element, chromium, and vanadium deposits in mafic and ultramafic rocks. *Econ Geol* 100th Anniversary, 215–249
- Chan LH, Edmond JM, Thompson G, Gillis K (1992) Lithium isotopic composition of submarine basalts: implications for the lithium cycle in the oceans. *Earth Planet Sci Lett* 108:151–160
- Cooper RW (1990) Distribution, occurrence, and crystallization of chromite and olivine in the lowermost Peridotite Zone, Stillwater Complex, Montana. In: *Lunar and Planetary Science Conference*, vol 21
- Cooper RWL (1997) Magmatic unconformities and stratigraphic relations in the Peridotite Zone, Stillwater Complex, Montana. *Can J Earth Sci* 34:407–425
- Dunn T (1986) An investigation of the oxygen isotope geochemistry of the Stillwater Complex. *J Petrol* 27:987–997
- Eggins SM, Rudnick RL, McDonough WF (1998) The composition of peridotites and their minerals: a laser-ablation ICP-MS study. *Earth Planet Sci Lett* 154:53–71
- Eiler JM, Farley KA, Valley JW, Stolper EM, Hauri EH, Craig H (1995) Oxygen isotope evidence against bulk recycled sediment in the mantle sources of Pitcairn Island lavas. *Nature* 377:138
- Eiler JM (2001) Oxygen isotope variations of basaltic lavas and upper mantle rocks. In: Valley JW, Cole DR (eds) *Stable isotope geochemistry, reviews in mineralogy*, vol 43. Mineralogical Society of America, Chantilly, Virginia, pp 319–364
- Elliott T, Thomas A, Jeffcoate A, Niu Y (2006) Lithium isotope evidence for subduction-enriched mantle in the source of mid-ocean-ridge basalts. *Nature* 443:565–568
- Horan MF, Morgan JW, Walker RJ, Cooper RW (2001) Re-Os isotopic constraints on magma mixing in the Peridotite Zone of the Stillwater Complex, Montana, USA. *Contrib Miner Petrol* 141:446–457
- Howland AL, Garrels EM, Jones WR (1949) Chromite deposits of Boulder River area, Sweetgrass County. US Government Printing Office, Montana

- Ireland RHP, Penniston-Dorland SC (2015) Chemical interactions between a sedimentary diapir and surrounding magma: evidence from the Phepane Dome and Bushveld complex, South Africa. *Am Miner* 100:1985–2000
- Irvine TN (1967) Chromian spinel as a petrogenetic indicator. Part II. Petrological applications. *Can J Earth Sci* 4:71–103
- Irvine TN (1975) Crystallization sequences in the Muskox intrusion and other layered intrusions II. Origin of chromitite layers and similar deposits of other magmatic ores. *Geochim Cosmochim Acta* 39:991–1020
- Irvine TN (1980) Magmatic density currents and cumulus processes. *Am J Sci* 280-A:1–58
- Jackson ED (1961) Primary textures and mineral associations in the Ultramafic Zone of the Stillwater Complex. Geological Survey Professional Paper, Montana. U.S
- Jackson ED (1969) Chemical variation in coexisting chromite and olivine in chromitite zones of Stillwater Complex. *Econ Geol* 4:41–71
- Jackson ED (1970) The cyclic unit in layered intrusions: a comparison of a repetitive stratigraphy in the ultramafic parts of the Stillwater, Muskox, Great Dyke and Bushveld complexes. In: Bushveld igneous complex and other layered intrusions, Symposium. Special Publication, Geological Society of South Africa, Johannesburg, South Africa, pp 391–424
- Jenkins MC, Mungall JE (2018) Genesis of the Peridotite Zone, Stillwater Complex, Montana, USA. *J Petrol* 59:2157–2189
- Johan Z, Martin RF, Ettler V (2017) Fluids are bound to be involved in the formation of ophiolitic chromite deposits. *Eur J Mineral* 29:543–555
- Jones WR, Peoples JW, Howland AL (1960) Igneous and tectonic structures of the Stillwater Complex, Montana. U.S. Geological Survey Bulletin 1071-H, 281–340
- Kaufmann FE, Vukmanovic Z, Holness MB, Hecht L (2018) Orthopyroxene oikocrysts in the MG1 chromitite layer of the Bushveld Complex: implications for cumulate formation and recrystallisation. *Contrib Miner Petrol* 173:17
- Lambert DD, Simmons EC (1987) Magma evolution in the Stillwater Complex: I. Rare-earth element evidence for the formation of the ultramafic series. *Am J Sci* 287:1–32
- Latypov RM, Chistyakova SY, Alapieti TT (2008) Infiltration metasomatism in layered intrusions revisited: a reinterpretation of compositional reversals at the base of cyclic units. *Mineral Petrol* 92:243–258
- Lenaz D, Garuti G, Zaccarini F, Cooper RW, Princivalle F (2012) The Stillwater Complex chromitites: The response of chromite crystal chemistry to magma injection. *Geol Acta* 10:33–41
- Li XH, Long WG, Li QL, Liu Y, Zheng YF, Yang YH, Chamberlain KR, Wan DF, Guo CH, Wang XC, Tao H (2010) Penglai zircon megacryst: a potential new working reference for microbeam analysis of Hf-O isotopes and U-Pb age. *Geostand Geoanal Res* 34:117–134
- Lipin BR (1993) Pressure increases, the formation of chromite seams, and the development of the ultramafic series in the Stillwater Complex, Montana. *J Petrol* 34:955–976
- Maier WD, Barnes SJ, Groves DI (2012) The Bushveld Complex, South Africa: formation of platinum–palladium, chrome- and vanadium-rich layers via hydrodynamic sorting of a mobilized cumulate slurry in a large, relatively slowly cooling, subsiding magma chamber. *Miner Deposit* 48:1–56
- Mattey D, Lowry D, Macpherson C (1994) Oxygen isotope composition of mantle peridotite. *Earth Planet Sci Lett* 128:231–241
- Matveev S, Ballhaus C (2002) Role of water in the origin of podiform chromitite deposits. *Earth Planet Sci Lett* 203:235–243
- McBirney AR, Noyes RM (1979) Crystallization and layering of the Skaergaard intrusion. *J Petrol* 20:487–554
- McCallum IS (1996) The Stillwater Complex. *Develop Petrol* 15(606):441–483
- McCallum IS (2002) The Stillwater Complex: a review of the geology. In: Stillwater Complex geology and guide: Billings, Montana, 9th International Platinum Symposium, vol 21, p 25
- McDonald JA (1965) Liquid immiscibility as one factor in chromitite seam formation in the Bushveld igneous complex. *Econ Geol* 60:1674–1685
- Mondal SK, Ripley EM, Li C, Ahmed AH, Arai S, Liipo J, Stowe C (2003) Oxygen isotopic compositions of Cr-spinels from Archean to Phanerozoic chromite deposits. *Geochim Cosmochim Acta Suppl* 67:301
- Mondal SK, Ripley EM, Li C, Frei R (2006) The genesis of Archean chromitites from the Nuasahi and Sukinda massifs in the Singhbhum Craton, India. *Precamb Res* 148:45–66
- Mondal SK, Mathez EA (2007) Origin of the UG2 chromitite layer, Bushveld Complex. *J Petrol* 48:495–510
- Mukherjee R, Mondal SK, Rosing MT, Frei R (2010) Compositional variations in the Mesoarchean chromites of the Nuggihalli schist belt, Western Dharwar Craton (India): potential parental melts and implications for tectonic setting. *Contrib Miner Petrol* 160:865–885
- Mungall JE, Kamo SL, McQuade S (2016) U-Pb geochronology documents out-of-sequence emplacement of ultramafic layers in the Bushveld igneous complex of South Africa. *Nat Commun* 7:13385
- O'Driscoll B, Donaldson CH, Daly JS, Emeleus CH (2009) The roles of melt infiltration and cumulate assimilation in the formation of anorthosite and a Cr-spinel seam in the Rum eastern layered intrusion, NW Scotland. *Lithos* 111:6–20
- Page P, Barnes SJ, Zientek ML (2011) Formation and evolution of the chromitites of the Stillwater Complex: a trace element study. In: Barra F (ed) Let's talk ore deposits: proceedings of the 11th SGA Biennial Meeting, Antofagasta, Chile. Society for Geology Applied to Mineral Deposits, pp 678–680
- Pebane M, Latypov RM (2017) The significance of magmatic erosion for bifurcation of UG1 chromitite layers in the Bushveld Complex. *Ore Geol Rev* 90:65–93
- Peoples JW, Howland AL (1940) Chromite deposits of the eastern part of the Stillwater Complex, Stillwater County. US Government Printing Office, Montana
- Raedeke LD, McCallum IS (1984) Investigations in the Stillwater Complex: Part II. Petrology and petrogenesis of the ultramafic series. *J Petrol* 25:395–420
- Richter FM, Davis AM, DePaolo DJ, Watson EB (2003) Isotope fractionation by chemical diffusion between molten basalt and rhyolite. *Geochim Cosmochim Acta* 67:3905–3923
- Rudnick RL, Ionov DA (2007) Lithium elemental and isotopic disequilibrium in minerals from peridotite xenoliths from Far-East Russia: product of recent melt/fluid-rock reaction. *Earth Planet Sci Lett* 256:278–293
- Schoenberg R, Zink S, Staubwasser M, Von Blanckenburg F (2008) The stable Cr isotope inventory of solid Earth reservoirs determined by double spike MC-ICP-MS. *Chem Geol* 249:294–306
- Schulte RF, Taylor RD, Piatak NM, Seal RR (2010) Stratiform chromite deposit model. U.S. Geological Survey Open-File Report
- Seitz HM, Woodland AB (2000) The distribution of lithium in peridotitic and pyroxenitic mantle lithologies—an indicator of magmatic and metasomatic processes. *Chem Geol* 166:47–64
- Spandler C, Mavrogenes J, Arculus R (2005) Origin of chromitites in layered intrusions: evidence from chromite-hosted melt inclusions from the Stillwater Complex. *Geology* 33:893–896
- Su BX, Chen C, Bai Y, Pang KN, Qin KZ, Sakyi PA (2017) Lithium isotopic composition of Alaskan-type intrusion and its implication. *Lithos* 286–287:363–368
- Su BX, Chen C, Pang KN, Sakyi PA, Uysal I, Avci E, Liu X, Zhang PF (2018) Melt penetration in oceanic lithosphere: Li isotope records

- from the Pozanti-Karsanti ophiolite in southern Turkey. *J Petrol* 59:191–205
- Su BX, Gu XY, Delouie E, Zhang HF, Li QL, Li XH, Vigier N, Tang YJ, Tang GQ, Liu Y, Brewer A, Mao Q, Ma YG (2015) Potential orthopyroxene, clinopyroxene and olivine reference materials for in situ lithium isotope determination. *Geostand Geoanal Res* 39:357–369
- Su BX, Zhang HF, Delouie E, Vigier N, Sakyi PA (2014) Lithium elemental and isotopic variations in rock-melts interaction. *Geochemistry* 74:705–713
- Su BX, Zhou MF, Jing JJ, Robinson PT, Chen C, Xiao Y, Liu X, Shi RD, Lenaz D, Hu Y (2019) Distinctive melt activity and chromite mineralization in Luobusa and Purang ophiolites, southern Tibet: constraints from trace element compositions of chromite and olivine. *Sci Bull* 64:108–121
- Su BX, Zhou MF, Robinson PT (2016) Extremely large fractionation of Li isotopes in chromitite-bearing mantle sequence. *Sci Rep* 6:22370
- Su BX, Robinson PT, Chen C, Xiao Y, Melcher F, Bai Y, Gu XY, Uysal I, Lenaz D (2020) The occurrence, origin and fate of water in chromitites in ophiolites. *Am Miner* 105:894–903
- Tang GQ, Li XH, Li QL, Liu Y, Ling XX, Yin QZ (2015) Deciphering the physical mechanism of the topography effect for oxygen isotope measurements using a Cameca IMS-1280 SIMS. *J Anal At Spectrom* 30:950–956
- Tang GQ, Su BX, Li QL, Xia XP, Jing JJ, Feng LJ, Martin L, Yang Q, Li XH (2019) High-Mg# olivine, clinopyroxene and orthopyroxene reference materials for in situ oxygen isotope determination. *Geostand Geoanal Res* 43:585–593
- Tomascak PB, Magna T, Dohmen R (2016) *Advances in Lithium Isotope Geochemistry*. Springer, Berlin
- Wager LR, Brown GM, Wadsorth WJ (1960) Types of igneous cumulates. *J Petrol* 1:73–85
- Xia J, Qin L, Shen J, Carlson RW, Ionov DA, Mock TD (2017) Chromium isotope heterogeneity in the mantle. *Earth Planet Sci Lett* 464:103–115
- Xiao Y, Teng FZ, Su BX, Hu Y, Zhou MF, Zhu B, Shi RD, Huang QS, Gong XH, He YS (2016) Iron and magnesium isotopic constraints on the origin of chemical heterogeneity in podiform chromitite from the Luobusa ophiolite. *Tibet Geochem Geophys Geosyst* 17:940–953
- Yang SH, Maier WD, Godel B, Barnes SJ, Hanski E, O'Brien H (2019) Parental magma composition of the Main Zone of the Bushveld Complex: evidence from in situ LA-ICP-MS trace element analysis of silicate minerals in the cumulate rocks. *J Petrol* 60:359–392
- Zientek ML, Czamanske, GK, Irvine TN (1985) Stratigraphy and nomenclature for the Stillwater Complex. In: Czamanske GK, Zientek ML (eds) *The Stillwater Complex, Montana: geology and guide*. Montana Bureau of Mines and Geology, Special Publication 92, pp 21–32